

BIOCOMPATIBLE NANOPARTICLES BASED ON AZA-BODIPY FOR
PHOTOTHERMAL THERAPY IN CANCER CELLS



A Thesis Submitted in Partial Fulfillment of the Requirements for the
Degree of Doctor of Philosophy in Chemistry
Suranaree University of Technology
Academic Year 2022

อนุภาคนาโนที่มีความเข้ากันได้ทางชีวภาพจากเอซาบอดีปี สำหรับการรักษา
แบบให้ความร้อนผ่านการกระตุ้นด้วยแสงในเซลล์มะเร็ง



นายศาสติญา คำแพงศรี

วิทยานิพนธ์นี้เป็นส่วนหนึ่งของการศึกษาตามหลักสูตรปริญญาวิทยาศาสตรดุษฎีบัณฑิต
สาขาวิชาเคมี
มหาวิทยาลัยเทคโนโลยีสุรนารี
ปีการศึกษา 2565

BIOCOMPATIBLE NANOPARTICLES BASED ON AZA-BODIPY FOR
PHOTOTHERMAL THERAPY IN CANCER CELLS

Suranaree University of Technology has approved this thesis submitted in
partial fulfillment of the requirements for the Degree of Doctor of Philosophy.

Thesis Examining Committee

Apiwat Chompoosor
(Assoc. Prof. Dr. Apiwat Chompoosor)

Chairperson

Anyanee Kamkaew
(Asst. Prof. Dr. Anyanee Kamkaew)

Member (Thesis Advisor)

James R. Cairns
(Prof. Dr. James R. Ketudat-Cairns)

Member

Theeranun Siritanon
(Assoc. Prof. Dr. Theeranun Siritanon)

Member

Rung-Yi Lai
(Asst. Prof. Dr. Rung-Yi Lai)

Member

KANTAPAT
(Dr. Kantapat Chansaenpak)

Member

Chatchai Jothityangkoon
(Assoc. Prof. Dr. Chatchai Jothityangkoon)

Vice Rector for Academic Affairs
and Quality Assurance

Santi Maensiri

(Prof. Dr. Santi Maensiri)
Dean of Institute of Science

ศาสติญา คำแพงศรี : อนุภาคนาโนที่มีความเข้ากันได้ทางชีวภาพจากเอซอบอดิปี สำหรับการ
การรักษาแบบให้ความร้อนผ่านการกระตุ้นด้วยแสงในเซลล์มะเร็ง (BIOCOMPATIBLE
NANOPARTICLES BASED ON AZA-BODIPY FOR PHOTOTHERMAL THERAPY IN
CANCER CELLS) อาจารย์ที่ปรึกษา : ผู้ช่วยศาสตราจารย์ ดร.อัญญาณี คำแก้ว, 59 หน้า

คำสำคัญ: อนุภาคนาโนจากพอลิเมอร์; เอซอบอดิปี; การรักษาโดยใช้ความร้อน; สารเรืองแสงในช่วง
อินฟราเรดช่วงคลื่นสั้น; เอซอบอดิปีนาโนเทคโนโลยีทางการแพทย์

การรักษาโดยใช้ความร้อนเป็นหนึ่งในวิธีที่ใช้ในการรักษาโรคมะเร็ง วัสดุนาโนที่มี
คุณสมบัติเชิงความร้อนภายใต้การถูกกระตุ้นด้วยแสง จะสามารถดูดซับและปลดปล่อยพลังงานที่ใกล้
ช่วงอินฟราเรดที่มีความยาวคลื่นในช่วง 750-900 นาโนเมตรได้ ซึ่งปัจจุบันได้รับความสนใจอย่างมาก
เนื่องจากการใช้วัสดุดังกล่าวสามารถแทรกซึมลงไปในส่วนลึกของเนื้อเยื่อชีวภาพได้ โดยทั่วไปแล้ว
วัสดุนาโนส่วนใหญ่จะถูกสร้างขึ้นจากการล้อมรอบหรือการเปลี่ยนพื้นผิวของวัสดุช่วยสร้างอนุภาคนา
โน ซึ่งวัสดุเหล่านี้ล้วนมีข้อจำกัดในเรื่องกระบวนการในการตรึงสารไว้ด้านในอนุภาคนาโน รวมถึง
ระยะเวลาในการเก็บรักษา ในงานวิจัยนี้ได้ทำการพัฒนาอนุภาคนาโนที่มีความเข้ากันได้ทางชีวภาพ
จากการใช้พอลิเมอร์ที่มีความเสถียร เชื่อมต่อกับเอซอบอดิปีผ่านทางพันธะเอไมด์ หลังจากนั้นจะเกิด
การก่อตัวเป็นอนุภาคนาโนเอซอบอดิปีเอ็มแพกซ์ขึ้นได้โดยธรรมชาติภายใต้สภาวะที่เหมาะสม ซึ่ง
อนุภาคนาโนที่ได้จะมีคุณสมบัติที่สูงในเรื่องของการละลายน้ำและการเข้ากันได้ทางชีวภาพในขณะที่
ยังสามารถคงคุณสมบัติในเชิงความร้อนของเอซอบอดิปีไว้เช่นเดิม ในการตรวจสอบคุณสมบัติของ
อนุภาคนาโนพบว่ามีความหนาแน่นเส้นผ่านศูนย์กลางประมาณ 170 นาโนเมตร และยังมีคุณสมบัติ
ของคุณสมบัติเชิงความร้อนรวมถึงสามารถใช้คุณสมบัติเชิงความร้อนนี้สำหรับการรักษาที่เชื่อมโยงทั้งใน
หลอดทดลองและในตัวอ่อนของสัตว์ทดลอง ในส่วนของการสกัดการไหลเวียนของโลหิตเข้าสู่
เซลล์มะเร็ง เพื่อยับยั้งกระบวนการสร้างหลอดเลือดใหม่ ๆ ของก้อนมะเร็ง และการต่อต้าน
เซลล์มะเร็งลำไส้ใหญ่ของมนุษย์ซึ่งถูกเพาะเลี้ยงไว้ในตัวอ่อนของไก่เพื่อใช้ในการทดลอง พบว่าอนุภา
คนาโนเอซอบอดิปีเอ็มแพกซ์มีประสิทธิภาพในการยับยั้งและการรักษาที่ดีกว่าเอซอบอดิปีประมาณ 30
เปอร์เซ็นต์ ดังนั้นในการวิจัยจึงคาดหวังว่าอนุภาคนาโนที่สังเคราะห์ขึ้นมีความเป็นไปได้ที่จะใช้ในการ
รักษาเซลล์มะเร็งของผู้ป่วยด้วยคุณสมบัติเชิงความร้อน

สาขาวิชาเคมี

ปีการศึกษา 2565

ลายมือชื่อนักศึกษา

ลายมือชื่ออาจารย์ที่ปรึกษา

ศาสติญา



SASTIYA KAMPAENGSRİ : BIOCOMPATIBLE NANOPARTICLES BASED ON AZA-BODIPY FOR PHOTOTHERMAL THERAPY IN CANCER CELLS. THESIS ADVISER : ASST. PROF. ANYANEE KAMKAEW, Ph.D. 59 PP.

Keywords: polymeric nanoparticles; aza-BODIPY; photothermal therapy; near-infrared photosensitizer; aza-BODIPY nanomedicine

Photothermal therapy is a cancer treatment. Photothermal nanomaterials can absorb and emit light in the near-infrared range (750–900 nm), which has drawn a lot of attention recently because of the deep penetration of NIR light in biological tissue. In general, most nanomaterials are produced by encapsulating or altering the surface of a nanoplatform that has limited loading capacity and long-term storage. Herein, we developed a biocompatible nanoparticle by using a stable polymer conjugated with aza-BODIPY via an amide bond that could self-assemble to form aza-BODIPY-mPEG nanoparticles. These particles demonstrated high efficiency for hydrophilicity and biocompatibility while retaining the dye's photothermal conversion characteristics. The nanoparticles had a hydrodynamic size of around 170 nm and exhibited great photostability and excellent photothermal therapy *in vitro* and *in ovo*. Aza-BODIPY-mPEG exhibited approximately 30% better anti-angiogenesis and antitumor activity against implanted xenograft human HCT116 tumor in the chick embryo when compared to parent aza-BODIPY-A. Altogether, this suggests that aza-BODIPY-mPEG is a promising material for cancer photothermal therapy.

School of Chemistry
Academic Year 2022

Student's Signature
Advisor's Signature

Sastiya
[Signature]

ACKNOWLEDGEMENTS

I would like to express my sincere thanks to my thesis advisor, Asst. Prof. Anyanee Kamkaew, and my collaborators because I received help, advice, and support. I would like to thank my advisor for consultation of research ideas and information. She always had time to discuss problems and results. I would like to thank everyone in the AK lab for giving me discussion, motivation, and creating a positive atmosphere in the laboratory.

I would like to thank Dr. Kantapat Chansaenpak, at the National Nanotechnology Center (Nanotec), a research institute under the National Science and Technology Development Agency (NSTDA), Thailand for advice and supporting me about this thesis. I would like to thank Dr. Chin Siang Kue at the Faculty of Health and Life Sciences, Management and Science University, Shah Alam, Selangor, Malaysia for study in chick embryo chorioallantoic membrane (CAM).

I would like to thank Prof. Dr. James R. Ketudat-Cairns and all International research network members for allowing me to use the tools for synthesis and characterization of nanoparticles. I would like to thank all lecturers in the School of Chemistry for teaching me. I would like to thank Thailand Science Research and Innovation for covering tuition, living costs, among other things. Finally, I would like to thank my family who supported me to develop into the person I am today for always supporting.

Sastiya Kampaengsri

CONTENTS

	Page
ABSTRACT IN THAI.....I	I
ABSTRACT IN ENGLISH.....II	II
ACKNOWLEDGEMENTS.....III	III
CONTENTS.....IV	IV
LIST OF TABLES.....VII	VII
LIST OF FIGURESVIII	VIII
LIST OF ABBREVIATIONSXI	XI
CHAPTER	
I INTRODUCTION..... 1	1
1.1 Research objectives.....5	5
1.2 Scope.....6	6
II LITERATURE REVIEW 6	6
2.1 Cancer disease.....6	6
2.2 Drug delivery by EPR effect8	8
2.3 Nanoparticles based on aza-BODIPY for phototherapy 11	11
2.4 Nano conjugation base polyethylene glycol..... 15	15
III RESEARCH METHODOLOGY 19	19
3.1 Materials and Instruments..... 19	19
3.2 Experimental Procedures 20	20
3.2.1 Synthesis of the aza-BODIPY derivative 20	20
3.3 Photophysical properties.....23	23
3.3.1 Particle characterization 23	23
3.3.2 Photothermal therapy..... 23	23
3.3.3 UV/NIR and fluorescence measurement..... 23	23
3.3.4 Fluorescent quantum yield..... 23	23

CONTENTS (Continued)

	Page
3.4 Cell culture and <i>In Vitro</i> assays.....	24
3.4.1 Photocytotoxicity.....	24
3.4.2 Live cell imaging.....	24
3.4.3 Live/dead cell staining.....	25
3.4.4 Flow cytometry	25
3.5 Chick embryo and <i>in ovo</i> toxicity.....	26
3.5.1 Chick embryo chorioallantoic membrane (CAM) model	26
3.5.2 Acute toxicity of NPs on chick embryo (<i>in ovo</i> toxicity).....	26
3.6 <i>In ovo</i> PTT study	26
3.6.1 Anti-angiogenesis.....	26
3.6.2 Grafting of HCT116 tumor cells in CAM and photothermal therapy.....	27
3.6.3 Tumor tissue histopathology analysis.....	27
IV RESULTS AND DISCUSSION	20
4.1 Synthesis and characterization of aza-BODIPY NPs.....	20
4.2 Photophysical properties of aza-BODIPY-mPEG NPs.....	35
4.3 Bio-applications of aza-BODIPY NPs.....	39
4.3.1 Live cell imaging.....	39
4.3.2 Photocytotoxicity	41
4.3.3 Live/dead cell staining.....	42
4.3.4 <i>In ovo</i> toxicity and anti-angiogenesis study.....	43
V CONCLUSION	52
REFERENCE.....	53
APPENDIX.....	61
CURRICULUM VITAE.....	62

LIST OF TABLES

Table	Page
1.1 Comparisons of aza-BODIPY nanocarrier for photothermal therapy.....	4



LIST OF FIGURES

Figure	Page
1.1	The self-assembly of aza-BODIPY-mPEG nanoparticles.....3
2.1	National ranking of cancer as a cause of death at ages <70.....7
2.2	Components of the multiphase tumor growth model.....8
2.3	Illustration of size effect on renal clearance and passive tumor targeting efficiency via EPR effect.....9
2.4	Illustration of the EPR effect at the site of injury.....10
2.5	Illustration of a tumor vessel illustrating loss of smooth muscle cells.....11
2.6	Illustration of the construction of BSA-Boca-BODIPY NPs for <i>in vivo</i> photoacoustic imaging-guided photothermal treatment.....12
2.7	Illustration of MAB NPs for imaging-guided synergistic PDT/PTT.....13
2.8	Illustration of the preparation of AZBNO ₂ @PCL.....13
2.9	Illustration of PAI and PTI guided PTT/PDT synergistic phototherapy with Xenon lamp irradiation using LABDP NPs.....14
2.10	Illustration of NAB NPs in weak acidic environment caused high rate of reactive oxygen species (ROS) generation.....15
2.11	Illustration of FMAB NPs for multimodal imaging guided PDT/PTT.....16
2.12	synthesis of 5FU-loaded Fa-polymer-auNP nanoconjugates.....17
2.13	Synthesis and molecular structure of Pa-PEG nanodots.....18
2.14	Radiation sensitivity of cancer cells can be enhanced after incubated with Fc-PEG nanoconjugates.....19
2.15	Reaction and formulation of covalent Ir820-Peg-diamine nanoconjugate.....20
3.1	Synthesis of aza-BODIPY-mPEG23
4.1	¹ H-NMR of compound 1.....32
4.2	¹³ C-NMR of compound 1.....33
4.3	¹ H-NMR of compound 2.....33
4.4	¹³ C-NMR of compound 2.....34

LIST OF FIGURES (Continued)

Figure	Page
4.5	¹ H-NMR of aza-BODIPY-A34
4.6	¹³ C-NMR of aza-BODIPY-A35
4.7	¹⁹ F-NMR of aza-BODIPY-A35
4.8	Comparison between ¹ H-NMR of aza-BODIPY-A , mPEG and aza-BODIPY-mPEG36
4.9	HRMS of aza-BODIPY-A37
4.10	MALDI-TOF MS of mPEG-COOH38
4.11	MALDI-TOF MS of aza-BODIPY-mPEG38
4.12	Synthesis of aza-BODIPY-mPEG39
4.13	Particle size of aza-BODIPY-A and aza-BODIPY-mPEG in water.....40
4.14	The hydrodynamic (HD) sizes of the NPs in various solutions.....41
4.15	Photophysical properties of aza-BODIPY-A in various solvents.....42
4.16	Absorbance of aza-BODIPY-A in DMSO and aza-BODIPY-mPEG in water, absorbance stability of aza-BODIPY-mPEG over time, heating curves of aza-BODIPY-mPEG with various concentrations.....43
4.17	Photothermal effect of the aqueous solution of the aza-BODIPY-mPEG45
4.18	Confocal images of MCF-7 treated with aza-BODIPY-mPEG and flow cytometry of MCF cells.....46
4.19	Confocal images of MCF-7 treated with aza-BODIPY-mPEG and colocalization images of aza-BODIPY-mPEG with Hoechst 33342.....47
4.20	The relative cell viability of MCF-7 under 808 nm at 5 min and fluorescent images of live/dead co-staining assay of MCF-7 cells.....48
4.21	Toxicity profile of mPEG-COOH , aza-BODIPY-A and aza-BODIPY-mPEG50
4.22	The temperature of the tumor tissue at different time point.....52
4.23	Human HCT116 tumor in CAM and percentage of HCT116 tumor volume changes across 3 days of observation.....53
4.24	Hematoxylin and eosin-stained tumor tissue at day 3 post-PTT.....54

LIST OF ABBREVIATIONS

AM	acetoxymethyl
Aza-BODIPY	Aza boron-dipyrromethene
Aza-BODIPY-A	Aza-BODIPY (free dye)
Aza-BODIPY-mPEG	Aza-BODIPY nanoparticle
CAM	Chick embryo chorioallantois membrane
DCM	Dichloromethane
DMSO	Dimethyl sulfoxide
EPR	Enhance permeability and retention
MeOH	Methanol
MTT	3-[4,5-dimethylthiazol-2-yl]-2,5 diphenyl tetrazolium bromide
NIR	Near infrared
NMR	Nuclear magnetic resonance
nm	Nanometer
NPs	Nanoparticles
PDT	Photodynamic therapy
PEG	Poly ethylene glycol
PI	Propidium iodide
PTT	Photothermal therapy

CHAPTER I

INTRODUCTION

Cancers are among the deadliest diseases on Earth (Y. Tang et al., 2019). Despite great efforts, cancer related deaths are still increasing. Innovative methods for better cancer treatment may be one answer. Currently most treatments rely on chemotherapy, surgery, or radiotherapy (Ferrari, 2005; Ma, Huang, Song, Chen, and Zhang, 2016; Ribas and Wolchok, 2018), which have side effects. Research also tries to develop a new way for cancer treatment. Novel treatment approaches to improve patient prognosis this is a fragment needs work (Phototheranostic; composed of optical diagnosis and phototherapy).

During the last four decades, research on the design and synthesis of smart photosensitizers for cancer therapy has emerged as a field. Real-time diagnosis and treatment systems has power and speed to correctly monitor cancer treatment. These systems provided enhanced efficacy and minimized side effects (skin phototoxicity, poor bioavailability and lack of tumor targeting) (X. Li et al., 2017). A newly developed technique using optical agents had shown highly effective to improve anti-cancer treatment. Researchers coined the term of Phototheranostics (Chen et al., 2020) consisting of diagnosis and therapy, including photodynamic therapy (PDT) and photothermal therapy (PTT). Owing to the unique properties of near-infrared absorption and emission, they showed high reactive oxygen species generation for PDT and photothermal conversion efficiency.

Phototherapies are a type of tumor-therapy that use fluorescent light or other sources of light, such as halogen lights, sunlight and light emitting diodes (LEDs) to treat tumors effectively in clinical cancer therapy. In the phototherapy process, the light irradiated and then activated non-toxic phototherapeutic agents (classified according to the reaction pathway involved in the cell death process), selectively in cancer cells without inducing severe side-effects (L. Hu et al., 2018; Xing et al., 2019). Moreover,

photothermal therapy (PTT) is one of phototherapy for cancer treatment which used optical radiation in the near infrared (NIR) wavelength range (700–2000 nm). When a laser was shined on a tissue, photons were absorbed by intercellular and intracellular areas and the energy of photons was converted into heat. As a result, the tissue temperature increased, leading to cell and tissue death (Cortezon-Tamarit et al., 2017).

Aza-boron-dipyrromethene (aza-BODIPY) and its derivatives are a new class of organic photosensitizers compared with traditional inorganic materials (e.g., TiO₂, ZnO). Aza-BODIPYs exhibited superior biocompatibility and intense red-shifted NIR absorbance (Jiang et al., 2015; Niu et al., 2009). They have better photostability compared with other organic photosensitizers (Awuah and You, 2012). They could enable flexible construction of desired photophysical characteristics, such as absorption/emission wavelength, singlet–triplet state and electrochemical characters. However, this photosensitizer family is usually hydrophobic with tumor-targeting abilities indicated the hydrophobic nature of this aza-BODIPY. Chemistry advances had allowed for modifying aza-BODIPY molecules by fabricating them into hydrophilic nano-assemblies; the modified aza-BODIPY could increase blood circulation to enhance accumulation in there tumor (Kamaly, Yameen, Wu, and Farokhzad, 2016; S. Li et al., 2018; Liang, Xu, Song, and Liu, 2016; Yamei Liu et al., 2019; Xing et al., 2019; Zou et al., 2017). A accumulation in tumors was observed to vary dramatically with particle size, cancer cell line and tumor location (Perry et al., 2017).

Nanoparticles (NPs) based on BODIPY dyes are a class of organic small molecules (diameter of particle has around 30 nm) and widely developed by encapsulating aza-BODIPY photosensitizers within functional amphiphilic polymers such as polyethylene glycol (PEG) (Chen et al., 2020) for cancer theranostics applications (Figure 1). The hydrophilic nanomedicines could select target tumor sites via an enhanced permeability and retention (EPR) effect. Nanoparticles in tumors had long stood as one of the fundamental principles of cancer drug delivery, which provide safe, simple and effective therapy. By allowing particles preferential access to tumors by advantage of size and longevity in circulation, EPR provided a neat rationale for the trend toward nano-sized drug carriers. Namely, in contrast to normal tissues and organs, most solid tumors showed a higher vascular density (hyper vasculature), i.e.,

angiogenesis that was one of the most important features of tumors to sustain their rapid growth (Iyer, Khaled, Fang, and Maeda, 2006; Hiroshi Maeda, Fang, Inutsuka, and Kitamoto, 2003). The blood vessels leak, due to rapid growth of new blood vessel allowing the nanoparticle to leak in the tumor tissue (H. Maeda, Bharate, and Daruwalla, 2009). Moreover, they showed deep-tissue fluorescence imaging and photoacoustic imaging, also optoelectronic property and easy functionalization (W. Hu et al., 2016; Ni et al., 2016; Q. Tang, Xiao, et al., 2017).

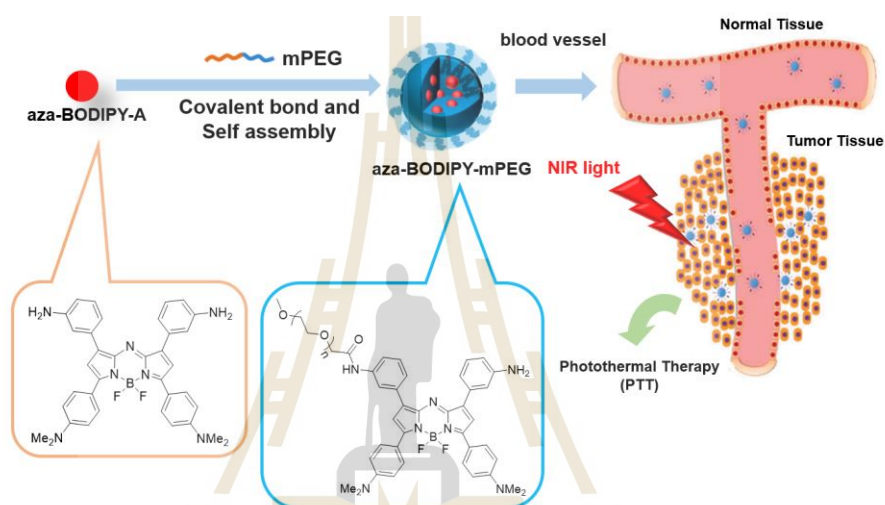


Figure 1.1 The self-assembly of aza-BODIPY-mPEG nanoparticles for the photothermal therapy at tumor sites.

For nanomedicine, two preliminary approaches formed aza-BODIPY NPs for cancer treatment. One was the encapsulation of aza-BODIPY with polymer via noncovalent bonds that from interactions of the organic dye throughout a polymeric matrix during formulation. The second loading strategy was the formulation of NPs by conjugation of polymer with aza-BODIPY via covalent bonds. The disadvantages of encapsulate NPs were burst release, low drug loading, large size distribution and difficulty of long-term storage. In addition, the conjugate NPS could be produced by regioselective synthesis, that is scalable, and give simple formulation, high drug loading-controlled release and storage in powder (Cohen, Yoshioka, Lucarelli, Hwang, and Langer, 1991).

In this study, we aimed to expose aza-BODIPY molecule with strong NIR absorption to a biocompatible nanoparticle by nano conjugation compared with nano encapsulation from previous work (Table 1). Finally, we synthesized **aza-BODIPY-A**, a dye with great NIR absorption and excellent photothermal conversion efficiency, and then coupled it with mPEG (Mn 5000) to create a biocompatible nanoparticle. This nano system has been tested both *in vitro* and *in ovo*.

Table 1.1 Comparisons of aza-BODIPY nanocarrier strategy for photothermal therapy within cancer cells.

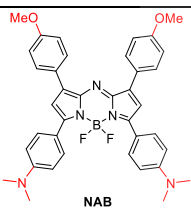
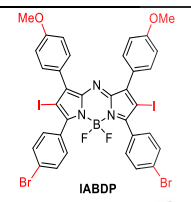
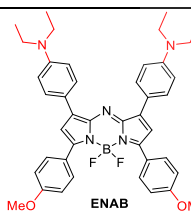
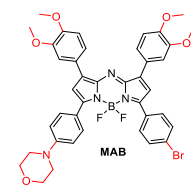
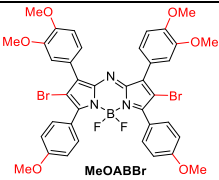
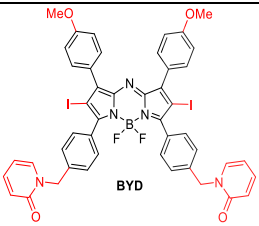
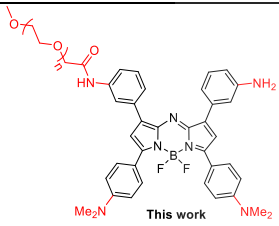
Aza-BODIPY	Polymer nanocarrier	Nanocarrier strategy	Application	Reference
	DSPE-mPEG	Encapsulation	Photo thermal therapy <i>in vitro</i> and <i>in vivo</i>	<i>Chem. Mater.</i> 2017 , 29, 5216–5224
	DSPE-mPEG	Encapsulation	Photo thermal therapy <i>in vitro</i> and <i>in vivo</i>	<i>J. Mater. Chem. B</i> , 2017 , 5, 1566-1573
	DSPE-mPEG	Encapsulation	Photo thermal therapy <i>in vitro</i> and <i>in vivo</i>	<i>Biomaterials</i> , 2019 , 221, 119422
	DSPE-mPEG	Encapsulation	Photo thermal therapy <i>in vitro</i> and <i>in vivo</i>	<i>ACS Appl. Bio Mater.</i> , 2019 , 2, 5888-5897

Table 1.1 Comparisons of aza-BODIPY nanocarrier strategy for photothermal therapy within cancer cells (Continued).

 <p>MeOABBr</p>	mPEG	Encapsulation	Photo thermal therapy <i>in vitro</i> and <i>in vivo</i>	<i>J. Mater. Chem. B</i> , 2018 , <i>6</i> , 4522-4530
 <p>BYD</p>	mPEG	Encapsulation	Photo thermal therapy <i>in vitro</i> and <i>in vivo</i>	<i>Biomaterials</i> , 2018 , <i>183</i> , 1–9
 <p>This work</p>	mPEG	Covalent conjugation	Photo thermal therapy <i>in vitro</i> and <i>in vivo</i>	This work

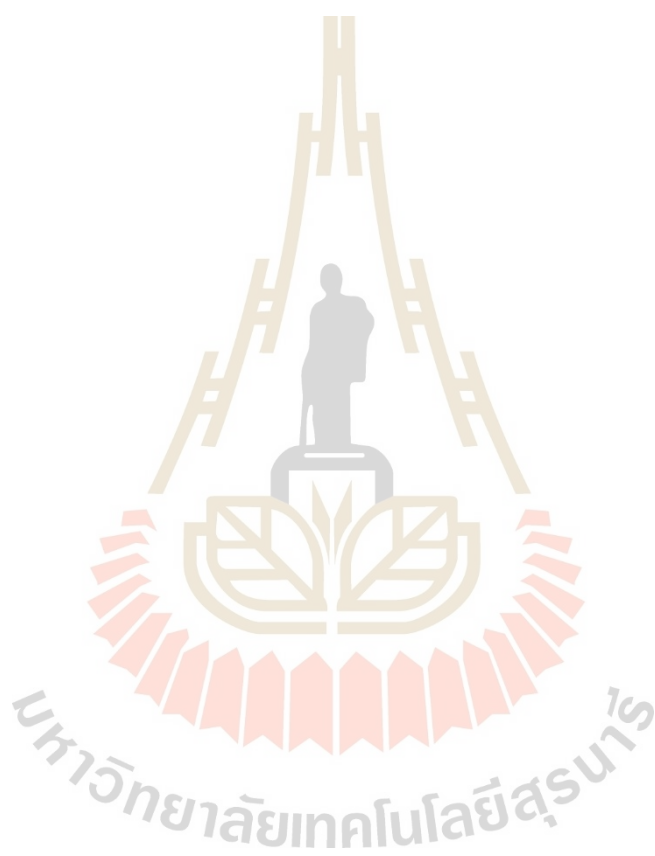
1.1 Research objectives

This project aimed to develop effective tumor targeted phototherapy probes that enhance cancer therapy with the following objectives:

- 1) To synthesize nanoparticles by conjugation of polyethylene glycol with aza-BODIPY to allow self-assembly of the nanoparticles.
- 2) To evaluate the photothermal conversion of the aza-BODIPY-PEG nanoparticle.
- 3) To investigate the photocytotoxicity by phototherapy effect of the designed molecules in cancer cells.

1.2 Scope

This project was synthesis and characterization of biocompatible nanoparticle by using a stable polymer conjugated with aza-BODIPY via amide bond that self-assembled to form **aza-BODIPY-mPEG** nanoparticles which used for cancer therapy.



CHAPTER II

LITERATURE REVIEW

2.1 Cancer disease

In the past, researchers had reported the occurrence of cancer disease worldwide. In the present, it has become one of determinant for cause of death (Ferrari, 2005). According to the data from the International Agency for Research on Cancer (Figure 2.1), the result showed about 18.1 million cancer causes in the world in 2018 and the number of deaths related with cancer diseases was 9.6 million in that year (Bray et al., 2018). The dangerous cancer motivated the development of technology for cancer treatment. Recently, the cancer therapies being used include surgery, chemotherapy, and radiotherapy (Curtin, 2012). However, surgery in many cases could scarcely remove all cancer cells, and both chemotherapy and radiotherapy might have severe side effects on normal cells (Curtin, 2012) In this literature review, effective therapies are presented achieve satisfactory treatment outcomes.

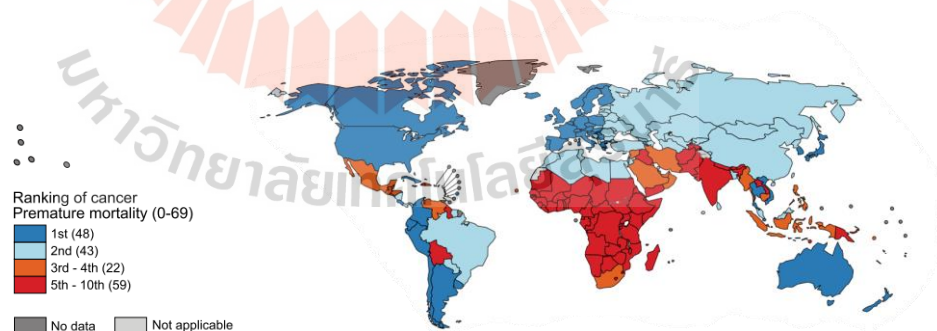


Figure 2.1 National Ranking of Cancer as a Cause of Death at Ages <70 Years in 2019. The numbers of countries represented in each ranking group are included in the legend. Copyright © 2012 Nature Reviews Cancer (Curtin, 2012).

2.2 Drug delivery by the enhanced permeability and retention (EPR) effect

Wirthl and coworker prepared the investigation of the interplay between the size of vessel-wall pores, the permeability of the blood-vessel endothelium and the lymphatic drainage on the delivery of particles of different sizes (Figure 2.2). Solid tumors developed a non-perfused core and increased interstitial pressure. They reported that two typical features of solid tumors limit nanoparticle delivery (Wirthl, Kremheller, Schrefler, and Wall, 2020). Only in case of small nanoparticles was the transport dominated by diffusion, and particles could reach the entire tumor. The size of the vessel-wall pores and the permeability of the blood-vessel endothelium had a major impact on the amount of delivered nanoparticles.

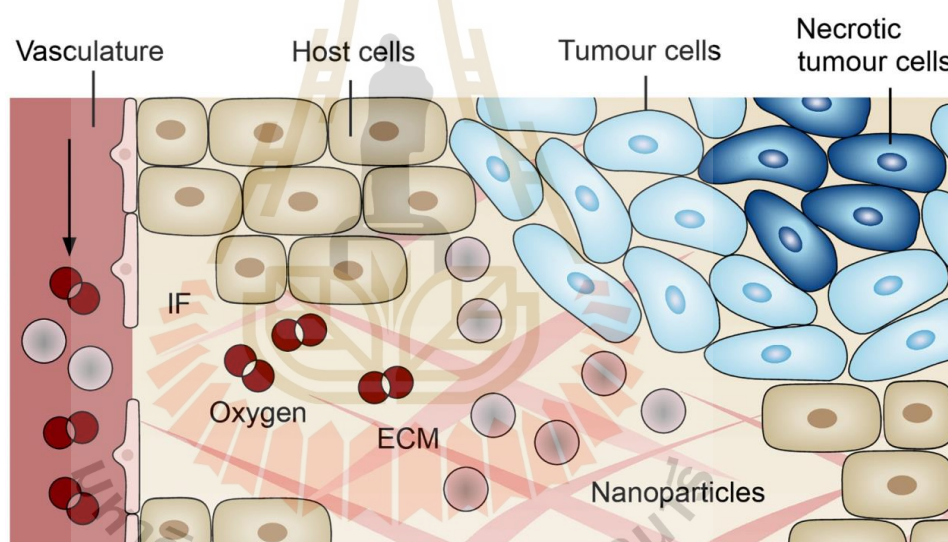


Figure 2.2 Components of the multiphase tumour growth model. The model comprises a solid phase, the ECM, three fluid phases, host cells, tumour cells and interstitial fluid (IF), and the vasculature which is modelled as an independent porous network. Copyright © 2020 Plos One (Wirthl et al., 2020).

Kang and coworker presented the size dependent the enhanced permeability and retention (EPR) effect of polymeric nanoparticles on tumor targeting using polyethylene glycol (PEG) in terms of their pharmacokinetics, biodistribution, and clearance (Kang et al., 2020). They reported small-sized polymeric NPs (<12 nm) could target tumor sites by the EPR effect, and renal clearance of administrated NPs

enhances tumor-to-background ratio (TBR) and reduces potential toxicity. As the MW of PEGs increased from 1 to 60 kDa, the elimination half-life and the area-under-the-curve (AUC) values increased proportionally. PEGs smaller than 12 nm showed minimal nonspecific uptake, while larger PEGs accumulated in major organs such as the lungs, liver, and pancreas with prolonged systemic circulation (Figure 2.3).

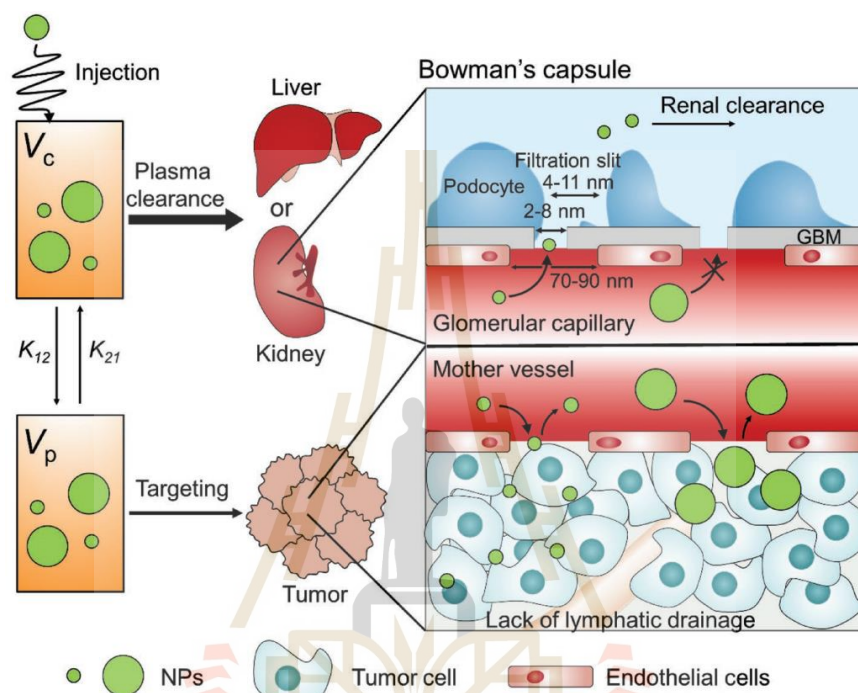


Figure 2.3 Illustration of size effect on renal clearance and passive tumor targeting efficiency via EPR effect. Copyright © 2020 Wiley Online Library (Kang et al., 2020).

Liu and coworker synthesized PLGA nanoparticles to accumulate at cancer cells (Figure 2.4). The mechanism of the permeability of the capillaries was investigated by local injection of histamine within blood vessel (Yingjun Liu et al., 2020). Moreover, they validated that the polymeric nanoparticles could directly migrate to the injured site without capture of immune cells in non-infected wound. While the infected wound allowed more nanoparticles to accumulate there due to the phagocytosis of local immune cells. The result showed the potential mechanism of “EPR effect” at the injured site. By loading with antibiotics, they demonstrated a new strategy for prevention of infection at the site of injury.

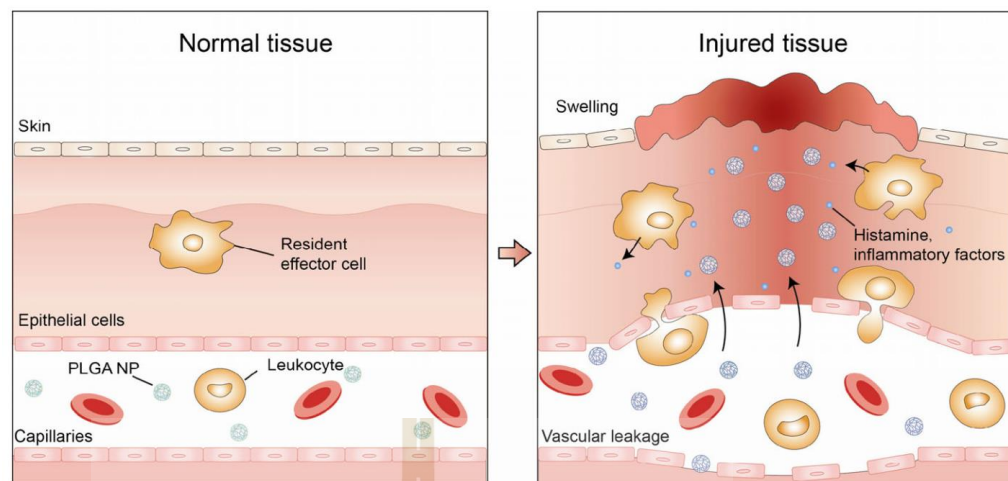


Figure 2.4 Illustration of the EPR effect at the site of cancer cells compared between normal tissue and injured tissue. The blood vessels could dilate and leak due to releasing of histamine to cause immune cells as well as nanoparticles to enter the injured tissue by passing out of the small blood vessels. Copyright © 2020 Springer Link (Yingjun Liu et al., 2020).

Wong and coworker presented a pharmacokinetic model to quantitatively assess the influence of the EPR effect on the uptake of a drug into a solid tumor (Figure 2.5). They used pharmacokinetic data for Doxil and doxorubicin from human clinical trials to illustrate how the EPR effect influences tumor uptake (Wong, Ye, Ulmschneider, and Searson, 2015). This work represented the process in quantitative analysis of accumulation of a drug or nanomedicine in tumor cells by the EPR effect. Also, represented are process as of drug delivery for cancer therapy that aren't the crucial EPR effect. Moreover, pharmacokinetic data of Doxil and doxorubicin showed mechanism of EPR effect which related with tumor accumulation for different values of the rate constants for tumor uptake by the EPR effect and intravasation back into circulation.

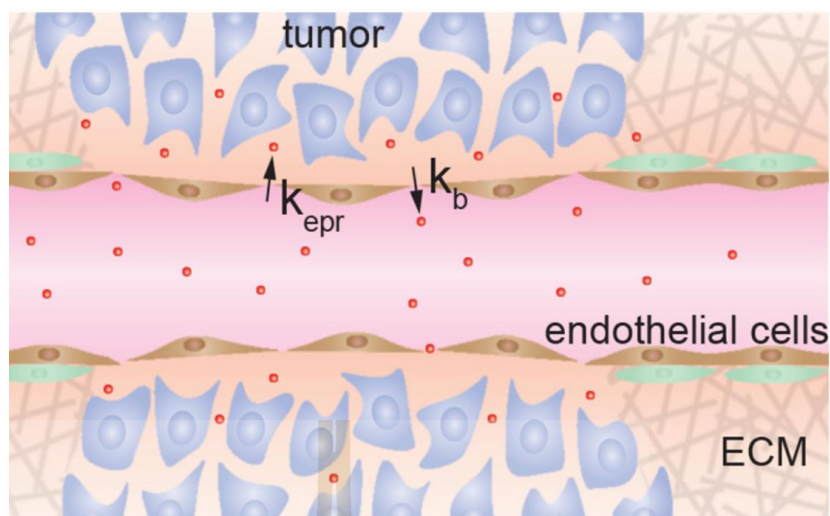


Figure 2.5 Illustration of a tumor vessel illustrating loss of smooth muscle cells, local degradation of the extracellular matrix, and increased permeability of the endothelium. Copyright © 2015 Plos One (Wong et al., 2015).

2.3 Nanoparticles based on aza-BODIPY for phototherapy

Aza-BODIPY dyes for cancer cells could obtain from many syntheses. Researchers tried to synthesize through various encapsulations for a lot of applications (photodynamic therapy, photothermal therapy, fluorescence imaging and photoacoustic imaging) (Gao et al., 2019). Gao group designed a theranostic agent with a simple molecular engineering (**BSA-Boca-BODIPY NPs**) where heavy atoms and alkyl chains promoted tumor theranostics. The **Boca-BODIPY** molecules further encapsulate with hydrophilic polymer through self-assembly water soluble and pass-through blood vessels to tumors (Figure 2.6).

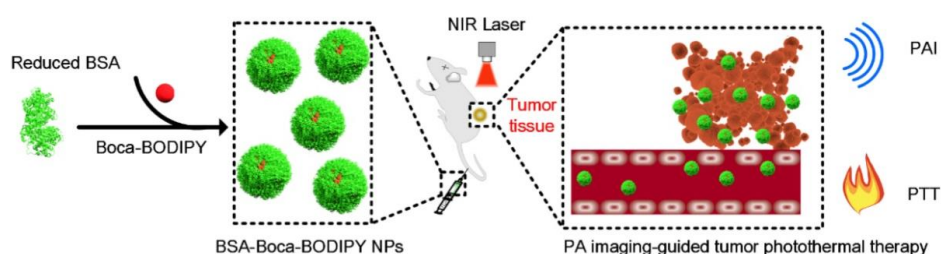


Figure 2.6 Illustration of the construction of **BSA-Boca-BODIPY NPs** for *in vivo* photoacoustic imaging-guided photothermal treatment. Copyright © 2019 Theranostics (Gao et al., 2019).

Tang and coworker reported aza-BODIPY organic photosensitizer that was **MAB**. The organic photosensitizer **MAB** with morpholine at the periphery site showed strong NIR absorption peak around 800 nm (Y. Tang et al., 2019) and had high pH sensitivity (pH change affect absorption, emission and phototherapy properties). In addition, the resulting structure favors the photoinduced electron transfer (PET) process: quenching a proton under weak acidic in tumor microenvironment (TME). And it could along with amplifying fluorescence and fortifying photothermal conversion efficiency as well as increasing reactive oxygen species (ROS). The encapsulation of **MAB** molecules with amphiphilic DPSE created biocompatible **MAB** nanoparticles (Figure 2.7).

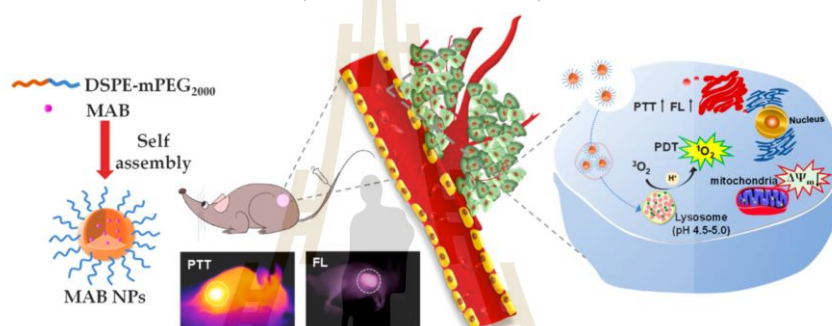


Figure 2.7 Illustration of **MAB NPs** for Imaging-Guided Synergistic PDT/PTT. Copyright © 2019 American Chemical Society (Y. Tang et al., 2019).

Chansaenpak group prepared water soluble, biodegradable, and biocompatible aza-BODIPY (**AZB-NO₂**) based polymeric NPs using the emulsification solvent evaporation method (Chansaenpak et al., 2018). They synthesized aza-BODIPY nanoparticles by encapsulated with polymer. Optical properties and applications of the organic NPs were capable of cancer cell imaging (Figure 2.8).

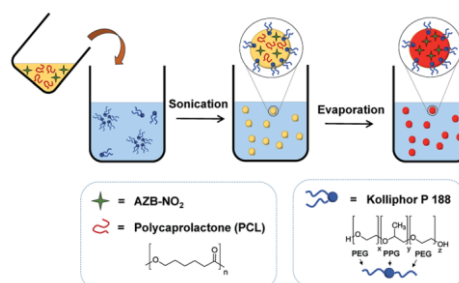


Figure 2.8 Illustration of the preparation of **AZBNO₂@PCL**. Copyright © 2018 Royal Society of Chemistry (Chansaenpak et al., 2018).

(Q. Tang, Si, et al., 2017) designed and synthesized biocompatible, near infrared absorbing and multi-functional photosensitizers, responding to tumor-specific signals for enhanced anticancer efficacy. It was a challenge of aza-BODIPY synthetic for tumor phototherapy (Figure 2.9). Moreover, a BF_2 chelate of [4-iodo-5-(4-bromophenyl)-3-(4-methoxyphenyl)-1H-pyrrol-2-yl][4-iodo-5-(4-bromophenyl)-3-(4-methoxyphenyl)pyrrol-2-ylidene]amine (**IABDP**) had high selective activation in intracellular lysosomes. In the acidic microenvironment in tumor tissues, **LABDH** could exhibit high rate of singlet oxygen generation efficiency at $\sim 92\%$.

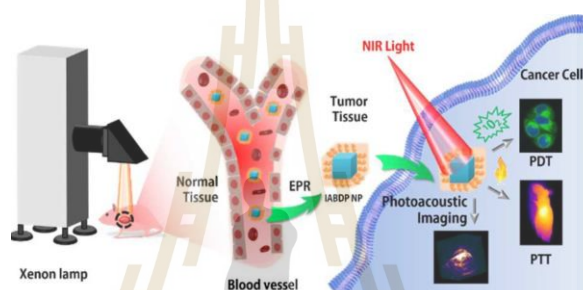


Figure 2.9 Illustration of PAI and PTI guided PTT/PDT synergistic phototherapy with Xenon lamp irradiation using **LABDP NPs**. Copyright © 2017 Royal Society of Chemistry (Q. Tang, Si, et al., 2017).

Qianyun Tang and coworker synthesized aza-BODIPY (NAB) which was pH-sensitive photosensitizer via nano-encapsulated for cancer therapy (Q. Tang, Xiao, et al., 2017). For nanoparticles synthetic, NAB was reacted with amphiphilic DSPE-mPEG₂₀₀₀ became NAB nanoparticles. the NPs presented diameter around 30 nm which had strong near-infrared absorption (~ 792 nm). NAB NPs could be activated in weak acidic environment. The results showed high rate of reactive oxygen species (ROS) generation and enhanced photothermal effect (Figure 2.10). The accumulation of NAB NPs in the lysosomes of tumor cells was activated under acidic microenvironment at pH 5.0 to produce ROS for photodynamic therapy via the photoinduced electron transfer (PET).

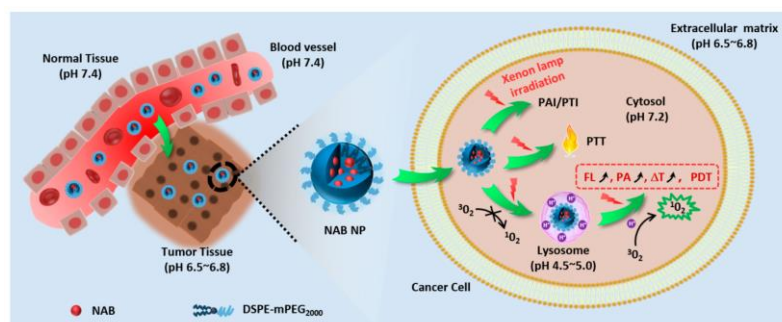


Figure 2.10 Illustration of NAB NPs in weak acidic environment caused high rate of reactive oxygen species (ROS) generation and enhanced photothermal effect. Copyright © 2019 American Chemical Society (Q. Tang, Xiao, et al., 2017).

The near-infrared (NIR) aza-BODIPY derivative (**MeOABBr**) was designed and synthesized by encapsulating with polyethylene glycol-folic acid (PEG-FA) and polyethylene glycol-triphenylphosphonium (PEG-TPP) to obtain dual targeting nanoparticles; tumor and mitochondria (**FMAB NPs**) (Chen et al., 2018). The organic photosensitizer (**FMAB**) showed great potential for tumor phototheranostics (Figure 2.11). Moreover, the photosensitizer with hydrophilic nanomedicines was selectively for target tumor sites via an enhanced permeability and retention effect. Triggered by NIR irradiation, **FMAB NPs** could generate ROS and hyperthermia causing mitochondrial failure resulting in cell apoptosis which was programmed cell death (Carneiro and El-Deiry, 2020).

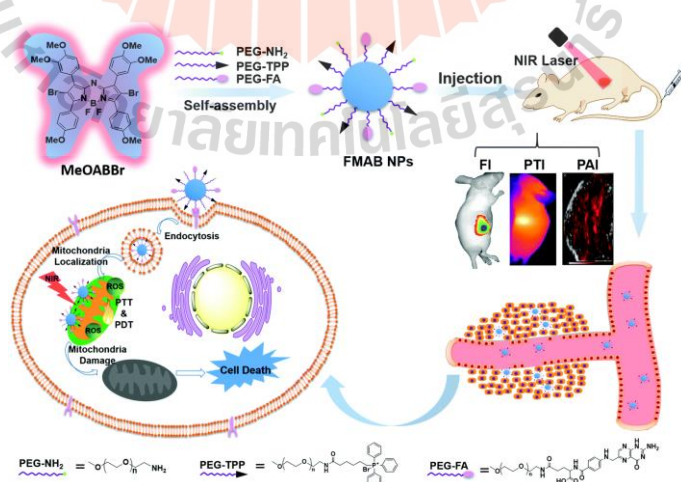


Figure 2.11 Schematic illustration of **FMAB NPs** for multimodal imaging guided PDT/PTT. Copyright © 2020 Journal of Materials Chemistry B (Carneiro and El-Deiry, 2020).

2.4 Nano conjugation based on poly ethylene glycol

Gajendiran and coworker synthesized AuNPs by using di- or tri-carboxylate-polyethylene glycol (PEG) polymers, including citrate-PEG (CPEG), malate-PEG (MAP), and tartrate-PEG (TAP), as a reducing and stabilizing agent (Gajendiran, Jo, Kim, and Balasubramanian, 2019). Polymer-AuNPs, the freely available hydroxyl and carboxylate groups of CPEG, MAP, and TAP were used to attach a cancer cell-targeting agent, FA, via a 1-Ethyl-3-(3-dimethylaminopropyl) carbodiimide/N-hydroxy succinimide coupling reaction to obtain FA-CPEG-AuNP, FA-MAP-AuNP, and FA-TAP-AuNP nanoconjugates, respectively. The result confirmed that AuNPs attached to CPEG, MAP, or TAP via the formation of π back bonding between AuNPs and the ester carbonyl group. The π back-bonded nanoconjugates exhibited sustained release of 5FU up to 27 days. FA-MAP-AuNPs exhibited an IC₅₀ at 5 $\mu\text{g}/\text{mL}$, while FACPEG-AuNPs and FA-TAP-AuNPs showed the IC₅₀ at 100 $\mu\text{g}/\text{mL}$ toward MCF-7 cancer cells (Figure 2.12).

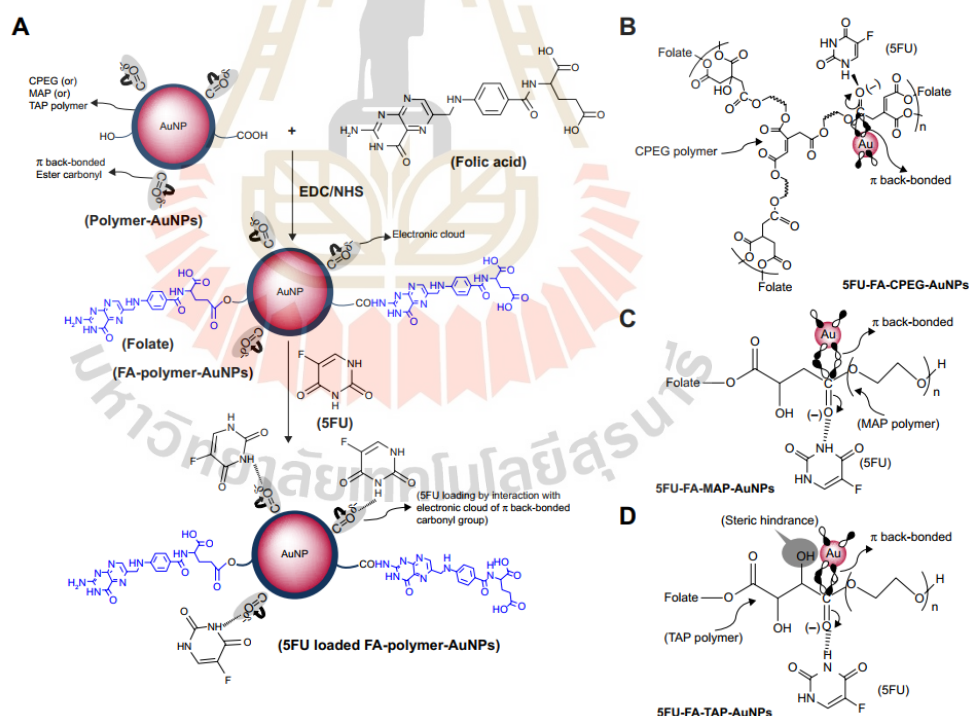


Figure 2.12 (A) synthesis of 5FU-loaded Fa-polymer-auNP nanoconjugates, graphical representation of (B) 5FU-loaded Fa-cPeg-auNP, (C) 5FU-loaded Fa-MaP-auNP, and (D) 5FU-loaded Fa-TaP-auNP nanoconjugates. Copyright © 2019 International Journal of Nanomedicine (Gajendiran et al., 2019).

Siwawannapong and coworker prepared Pa-PEG nanodots. The nanoparticle was synthesized by using amide coupling reaction of PEG-NH₂ and Pa-COOH to generate ultra-small nanodots. The characterization showed particle size from TEM around 2 nm (Siwawannapong et al., 2020). Also, the stability test of nanodots could present good stability in various physiological solutions. The nanoparticle was investigated by *in vitro* and the Pa-PEG nanodots showed remarkable potential to induce cytotoxicity against cancerous cells upon irradiation with a red LED lamp (Figure 2.13). Guidance by PA/FL dual imaging techniques, the optimal time for PDT treatment was suggested to be 8 h after intravenous (i.v.) injection. *In vivo* PDT conducted in 4T1 tumor-bearing mice exhibited great therapeutic efficacy under light irradiation with renal excretable behavior and no long-term side effects.

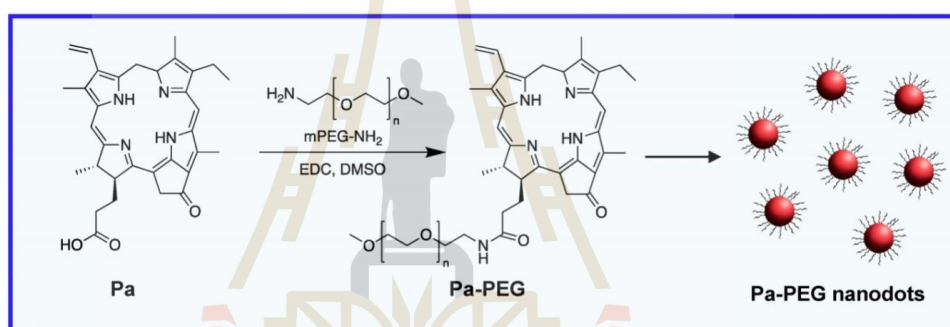


Figure 2.13 Synthesis and molecular structure of Pa-PEG nanodots. Copyright © 2020 Theranostics (Siwawannapong et al., 2020).

Tian and coworker prepared nanoparticle by the conjugation of ferrocene with poly ethylene glycol (Fc-PEG) (J. Tian et al., 2016), which used as possess the following characteristics: (i) one-step preparation in favorable yield, (ii) increased solubility of ferrocene molecule, and (iii) enhanced cellular uptake via formation of nanoscale aggregates. The chemical structure was characterized by various techniques. They also investigated the relationships of cellular uptake and intracellular reactive oxygen specimen (ROS) level with the apoptosis of cells. It was found that the higher atomic numbers (high-Z) effect of Fe elements accompanied by the alleviation of hypoxic anoxia of the cancer cells could improve their radiation sensitivity for promoting further potential clinical applications (Figure 2.14).

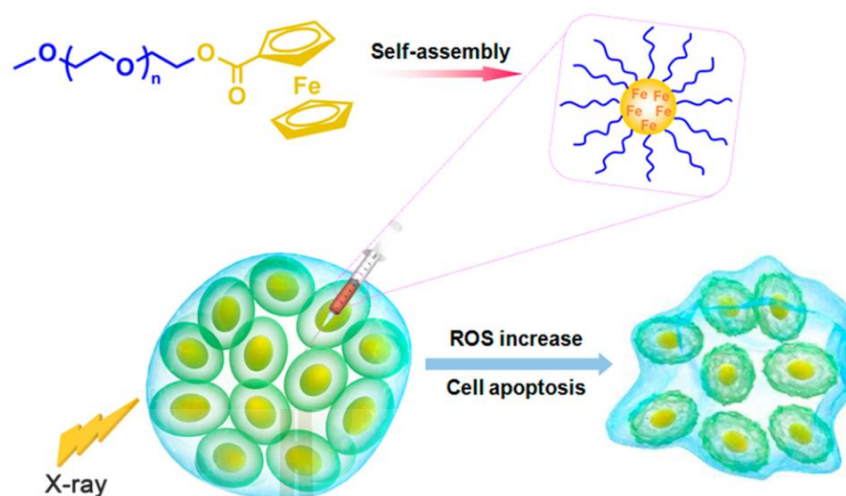


Figure 2.14 Radiation Sensitivity of Cancer Cells Can Be Enhanced after Incubated with Fe-PEG Nanoconjugates. Copyright © 2016 American Chemical Society (J. Tian et al., 2016).

Fernandez and coworker synthesized nanoconjugate (IRPDcov) for *in vivo* applications by using polyethylene glycol (PEG)-diamine conjugated with IR820 (Fernandez-Fernandez et al., 2014). The conjugation of nanoparticle displayed the particle size as a spherical which had diameter approximately 150 nm and zeta potential was -0.4 ± 0.3 mV. The nanoparticle presented fluorescent property and resulted to hyperthermia-mediated cell-growth inhibition. Also, the results showed ability for enhanced internalization and enhanced cytotoxic hyperthermia effects in cancer cells compared with free dye. Moreover, The nanoparticle provided a multifunctional delivery vector whose localization could be monitored with noninvasive techniques and that might also serve for guided hyperthermia cancer treatments (Figure 2.15).

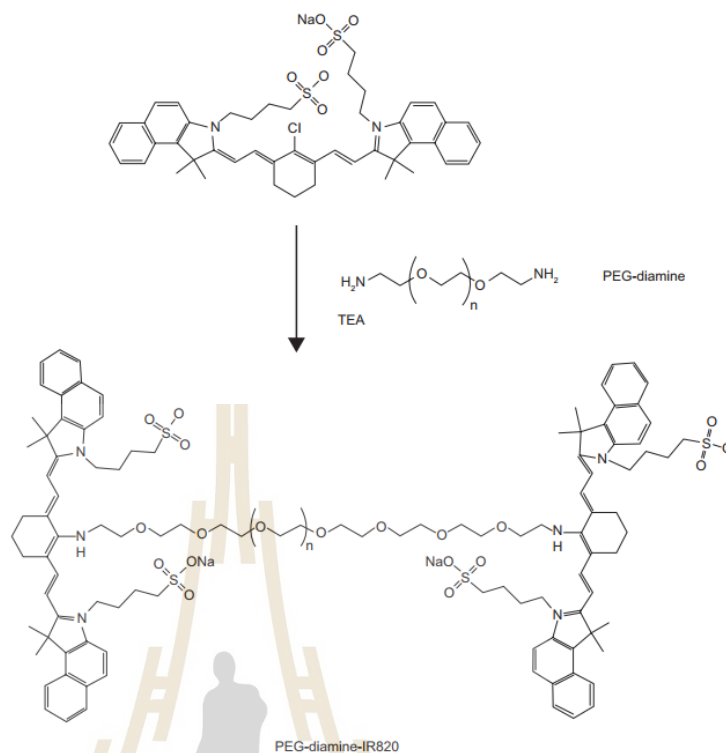


Figure 2.15 Reaction and formulation of covalent Ir820-Peg-diamine nanoconjugate (IRPDcov). Copyright © 2014 International Journal of Nanomedicine (Fernandez-Fernandez et al., 2014).

CHAPTER III

RESEARCH METHODOLOGY

3.1 Materials and Instruments

All glassware were oven-dried prior to use. All solvents and reagents were obtained of analytical grade from various manufactures (Sigma Aldrich, TCI, Carlo Erba, Acros and Merck). Aza-BODIPY-A was synthesized following the previous literature (Cheng, Maruani, Savoie, Chudasama, and Boyle, 2018). All reactions were monitored by thin-layer chromatography using silica gel (Carlo Erba) as the stationary phase and organic solvent (ethyl acetate and hexane from various manufactures) as the mobile phase. Analytical thin layer chromatography (TLC) was performed on TLC Silica gel 60 F254 (Merck) and visualize with a UV cabinet. All compounds were characterized by ^1H , ^{13}C nuclear magnetic resonance (NMR). The NMR spectra were recorded with a 500 MHz (^1H), 125 MHz (^{13}C), 470 MHz (^{19}F) NMR spectrometer (Avance III Spectrometer, Bruker biospin Ag, USA) using CDCl_3 or CD_3OD as a solvent reported in ppm using tetramethylsilane (TMS) as an internal standard. Molecular mass was measured under electrospray ionization condition (ESI, microtof Bruker biospin Ag, Germany) in positive mode. The physical properties of the aza -BODIPY-mPEG nanoparticle were investigated by dynamic light scattering (DLS) (Malvern Model Zetasizer-ZS), JEM-2100-Plus transmission electron microscope (TEM; JEOL), and SU-8030 field-emission scanning electron microscope (SEM; Hitachi). The concentration of the aza-BODIPY-mPEG nanoparticle was calculated from UV-vis-NIR absorbance by using aza-BODIPY-A calibration curve. UV-vis-NIR absorption spectra were monitored by the Cary Series UV-vis-NIR spectrophotometer (Agilent Tech, Santa Clara, CA, USA). The fluorescence spectra were recorded under the excitation wavelength at 750 nm by the PerkinElmer LS55 fluorescence spectrometer (PerkinElmer, USA) using a quartz cell of 1

cm path length. The photothermal property was monitored by using 808 nm laser (0.7 W/cm^2) for 10 min. Real-time temperature changes were recorded using a FLIR thermal camera and thermometer digital Nicety DT1311 K-type.

3.2 Experimental Procedures

3.2.1 Synthesizing the aza-BODIPY derivative:

aza-BODIPY-mPEG synthetic was presented in Figure 3.1. The synthesis starts from an Aldol condensation reaction between acetophenone (**1**) and aldehyde (**2**) to generate α,β -unsaturated ketone or chalcone (**3**). Then Michael addition reaction was used between chalcone and nitromethane (**4**). Ammonium acetate was used for coupling reaction become dipyrromethene (**5**). Pd/C with enough pressure of H_2 was used for hydrogenation (**6**). And then, boron complex to make the photosensitizer (**7**). Finally, this molecule was connected with polyethylene glycol by amide coupling reaction (**8**).

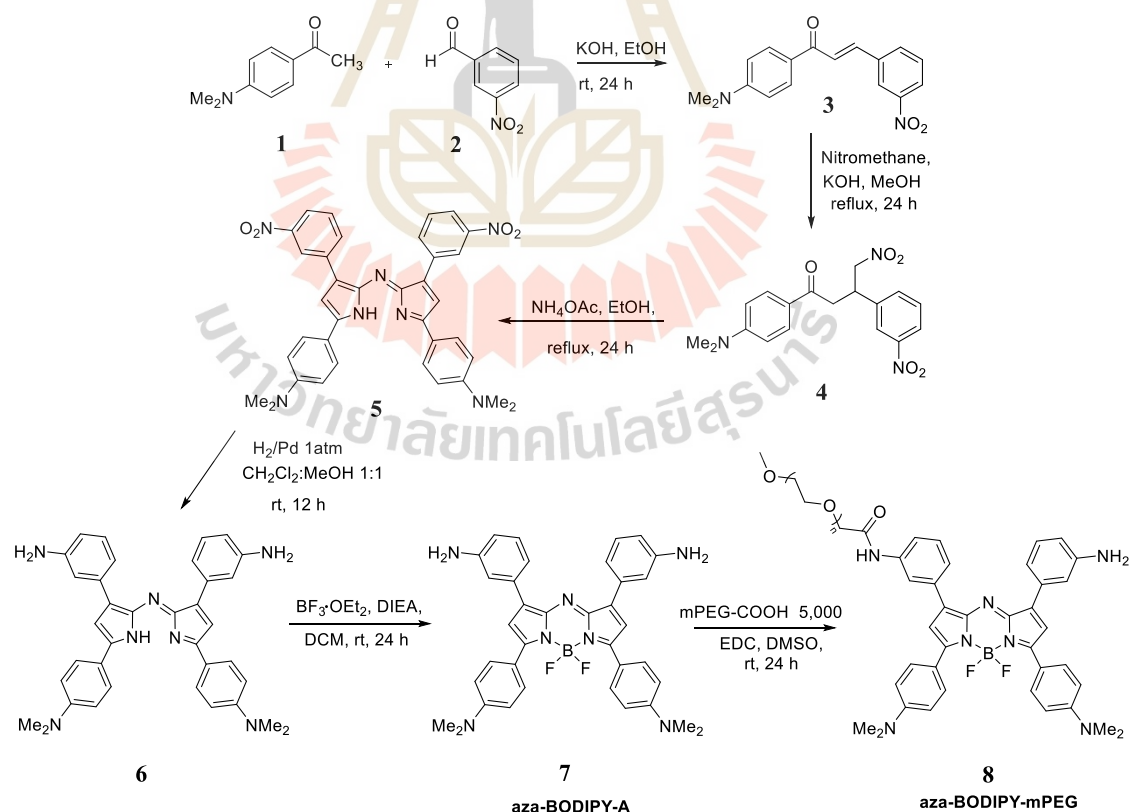


Figure 3.1 The synthesis of aza-BODIPY-mPEG.

3.2.1.1 (E)-1-(4-(dimethylamino)phenyl)-3-(3-nitrophenyl)prop-2-en-1-one

Firstly, chalcone derivative was synthesized by using aldehyde and ketone as starting materials. A solution of 4'-dimethylaminoacetophenone (**1**) in ethanol was added with potassium hydroxide and 3-Nitrobenzaldehyde (**2**) in ethanol respectively. The reaction was stirred at room temperature overnight. The Precipitate was filtered and washed with cold ethanol (4-6 °C). The product was obtained as a yellow solid (95% yield). ¹H NMR (500 MHz, CDCl₃) δ 8.50 (s, 1H), 8.22 (d, *J* = 8.0 Hz, 1H), 8.02 (d, *J* = 9.0 Hz, 2H), 7.90 (d, *J* = 7.5 Hz, 1H), 7.79 (d, *J* = 15.5 Hz, 1H), 7.69 (d, *J* = 15.5 Hz, 1H), 7.59 (t, *J* = 7.8 Hz, 1H), 6.75 (d, *J* = 8.5 Hz, 2H), 3.11 (s, 6H). ¹³C NMR (125 MHz, CDCl₃) δ 187.0, 153.7, 149.0, 139.6, 137.6, 134.3, 131.2, 130.0, 126.0, 125.1, 124.2, 122.2, 111.3, 40.4. ESI-HRMS (C₁₇H₁₆N₂O₃Na): calculated [M + Na]⁺: 319.1053, found: 319.1060.

3.2.1.2 1-(4-(dimethylamino)phenyl)-4-nitro-3-(3-nitrophenyl)butan-1-one

Potassium hydroxide was added to a solution of chalcone (**3**) in MeOH at room temperature. Nitromethane was added to the reaction mixture, and then the reaction was heated up to reflux at 78 °C for 24 h. After that, the reaction was cooled to room temperature, HCl was added to neutralize. Precipitate was filtered out and washed with cold MeOH. The product was obtained as a slightly brown solid (61% yield). ¹H NMR (500 MHz, CDCl₃) δ 8.18 (s, 1H), 8.13 (d, *J* = 8.0 Hz, 1H), 7.82 (d, *J* = 9.0 Hz, 2H), 7.67 (d, *J* = 7.5 Hz, 1H), 7.51 (t, *J* = 7.8 Hz, 1H), 6.67 (d, *J* = 9.0 Hz, 2H), 4.90 (dd, *J* = 12.5, 5.5 Hz, 1H), 4.73 (dd, *J* = 12.5, 8.5 Hz, 1H), 4.39 – 4.33 (m, 1H), 3.38 (dd, *J* = 6.5, 3.5 Hz, 2H), 3.07 (s, 6H). ¹³C NMR (125 MHz, CDCl₃) δ 193.7, 153.8, 148.8, 142.0, 134.5, 130.5, 130.1, 124.6, 123.0, 122.4, 111.3, 79.3, 40.5, 40.4, 39.4. ESI-HRMS (C₁₈H₁₉N₃O₅Na): calculated [M + Na]⁺: 380.1217, found: 380.1220.

3.2.1.3 (Z)-4-(2-((5-(4-(dimethylamino)phenyl)-3-(3-nitrophenyl)-1H-pyrrol-2-yl)imino)-3-(3-nitrophenyl)-2H-pyrrol-5-yl)-N,N-dimethylaniline

Ammonium acetate was added to the ethanol solution of structure (**4**). The reaction was heated up to reflux at 120 °C and stirred for 24 h. The mixture was

cooled to 40 °C, then the solvent was removed for increasing concentration. The residue was precipitated in cold EtOH, the solid was filtered yielding a dark solid purified with flash silica chromatography then eluted with CH₂Cl₂. The product was obtained as a green solid (65% yield).

3.2.1.4 (Z)-4-(3-(3-aminophenyl)-2-((3-(3-aminophenyl)-5-(4-(dimethylamino)phenyl)-1H-pyrrol-2-yl)imino)-2H-pyrrol-5-yl)-N,N-dimethylaniline

Previous substance (**5**) was dissolved in CH₂Cl₂: MeOH (1:1). Pd/C was added to the solution. The mixture was stirred under H₂ (1 atm) at room temperature for 20 h, the reaction was followed by TLC. The product was filtered through Celite® to give dark green solid after remove the solvent (94% yield).

3.2.1.5 (Z)-4-(3-(3-aminophenyl)-2-((3-(3-aminophenyl)-1-(difluoroboronyl)-5-(4-(dimethylamino)phenyl)-1H-pyrrol-2-yl)imino)-2H-pyrrol-5-yl)-N,N-dimethylaniline (aza-BODIPY-A)

The solid intermediate (**6**) was then dissolved in CH₂Cl₂. N, N-diisopropyl ethylamine was added to the solution. The mixture was stirred at room temperature for 20 minutes followed by added BF₃•OEt₂ in one portion and then stir for 12 h under nitrogen atmosphere. The reaction was quenched with water stirred vigorously for 15 min. The organic layer was separated and washed with HCl and brine solution. The organic layer was dried over anhydrous MgSO₄, filtered, and the solvent was removed under reduced pressure. The residue was purified by flash column chromatography eluting with EtOAc: Hexanes. The product was obtained as a purple solid (80% yield). ¹H NMR (500 MHz, CDCl₃) δ 7.98 (d, *J* = 9.0 Hz, 4H), 7.58 (s, 2H), 7.21 (d, *J* = 7.5 Hz, 2H), 7.08 (t, *J* = 8.0 Hz, 2H), 6.93 (s, 2H), 6.62 (d, *J* = 9.0 Hz, 4H), 6.61 (d, *J* = 5.5 Hz, 2H), 3.68 (s, 12H). ¹³C NMR (125 MHz, CDCl₃) δ 155.9, 151.7, 145.9, 144.9, 140.4, 133.8, 131.5, 129.1, 119.4, 119.0, 117.8, 116.8, 116.0, 111.8, 39.8. ¹⁹F NMR (470 MHz, CDCl₃) δ -131.89 (q, *J* = 31.9 Hz, BF₂). ESI-HRMS (C₃₆H₃₄BF₂N₇): calculated [M]⁺: 613.2937, found: 613.2997.

3.2.1.6 Aza-BODIPY-mPEG

Previous substance (**7**), methoxy polyethylene glycol carboxylic acid (mPEG-COOH) and 1-ethyl-3-(3-dimethylaminopropyl)- carbodiimide (EDC) were

dissolved in Dimethyl sulfoxide (DMSO). The reaction was stirred at room temperature for 24 h. The solution was diluted with H₂O and then stirred for dialysis in H₂O for 24 h. After dialysis step, the solution was sonicated and centrifuged then filtrated by filter molecular weight cut of 200 nm then stored at 4 °C (54% yield). The particle size of **aza-BODIPY-mPEG** was measured by Dynamic Light Scattering (DLS) technique. MALDI-TOF MS (C₃₆H₃₄BF₂N₇-mPEG-COOH): calculated [M + H]⁺: 5595, found: 5873.

3.3 Photophysical Properties

3.3.1 Particle characterization

The solution of nanoparticle was stocked in DI water. The physical properties of the aza-BODIPY-mPEG were investigated by dynamic light scattering (DLS) (Malvern Model Zetasizer-ZS), JEM-2100-Plus transmission electron microscope (TEM; JEOL), and SU-8030 field-emission scanning electron microscope (SEM; Hitachi).

3.3.2 Photothermal therapy

The solution of **aza-BODIPY-mPEG** with different concentration in DI water were irradiated with 808 nm laser (0.7 W/cm²) for 10 min. The temperature was recorded by FLIR thermal camera and digital thermometer. DI water was used as the control group. The real-time temperature change was recorded using a FLIR thermal camera and thermometer digital Nicety DT1311 K-type. All these results were demonstrated that **aza-BODIPY-mPEG** was suitable for *in vivo* photothermal therapy guided cancer therapy.

3.3.3 UV/NIR and fluorescence measurement

The solution of samples was stocked in DMSO. The NIR-UV-visible absorption was obtained Aligent CARY5000 (Aligent technology, USA). The fluorescence spectra were record at excitation wavelength of 780 nm and measured by Perkin Elmer LS55 (Perkin Elmer, USA) using a quartz cell of 1 cm path length.

3.3.4 Fluorescent quantum yield

Fluorescent quantum yield (Φ_f) was defined as the ratio of the number of photons released to the number of photons absorbed. Both the adsorption and

emission of fluorescence (780 nm excitation) spectra were measured for the dilution of **aza-BODIPY-mPEG** in DMSO, water and PBS.

3.4 Cell Culture and *In Vitro* Assays

For the human cancer cells including MDA-MB-231 (human breast cancer), MCF-7 (human breast cancer) and HeLa (human cervical cancer) were cultured in Dulbecco's Modified Eagle's Media (DMEM) and MCF-10A in Mammary Epithelial Basal Medium (MEBM) on 75 cm³ culture flasks supplemented with 10% fetal bovine serum (FBS) and 1% penicillin–streptomycin (P/S) under humidified 95% air, 5% CO₂ atmosphere at 37 °C.

3.4.1 Photocytotoxicity

After cell binding and cell internalization checking, MTT assay was investigated the photocytotoxicity of proposed compound. This technique was confirmed the Cancer cells destroyed which depended on **aza-BODIPY-mPEG** levels via PTT property. Approximately 7×10^3 cells of MDA-MB-231, MCF-7 and HeLa were seeded on 96-well cell culture plates per well and incubated in complete media for 24 h. All cells were treated with various concentration of **aza-BODIPY-mPEG** (0.1, 0.5, 1, 2.5, 5, 10, 20, 50 μM) for 4 h. Then, the cells were washed with PBS buffer for 3 times and then irradiated with without 808 nm lamp for 0.5 h. All the cells were cultured for further 24 h incubation. After 24 h, the cells were washed with PBS buffer for 3 times and treated with 0.5 mg mL⁻¹ of MTT solution in PBS buffer for 2 h. DMSO was added to dissolve formazan product which can detect through UV-vis absorption at wavelength 840 nm to quantify number of live cells. Number of the live cells could mean higher phototoxicity of the compounds.

3.4.2 Live cell imaging

MCF-7 cells 1×10^4 cells/well were seeded on an 8-well chambered cover glass (LabTek, Nunc) for 24 h. After that for the time-dependent experiment, the cells were treated with 5 μM of **aza-BODIPY-mPEG** for 0, 1, 4, 12, and 24 h. For the dose-dependent experiment, the cells were treated with 0, 2.5, and 5 μM of **aza-BODIPY-mPEG** for 4 h. Then, the cells were washed with PBS buffer (pH 7.4) twice before

incubating in medium containing 1.0 μM of Hoechst 33342 (DNA fluorescent staining, Thermo Fisher Scientific) and organelle trackers: 1.0 μM of LysoTracker Green DND-26 (Thermo Fisher Scientific), MitoTracker Green FM (Thermo Fisher Scientific), and C6-NBD Ceramide (Golgi tracker, Avanti Polar Lipids) for 10 min for colocalization experiments. A laser scanning confocal microscope (Nikon A1Rsi) with 643 nm laser (aza-BODIPY-mPEG) and 405 nm laser (Hoechst33342) were used to observe the cells under a 60x oil immersion objective lens.

3.4.3 Live/dead cell staining

To investigate both live and dead cells via photocytotoxicity were proved by using 1.5×10^3 cells of MDA-MB-231, MCF-7 and HeLa which were seeded in 35 mm glass-bottom confocal dishes and incubated in complete media for 24 h before staining. And all cells were treated with 5 μM of aza-BODIPY-mPEG for 4 h. After that, the cells were irradiated with 808 nm lamp light for 0, 1, 5, 10, 15, 20, 30 min to induce photocytotoxicity and then the dyes were washed out with PBS buffer for 3 times. The cells were stained with 5 μM of propidium iodide (PI) and 15 μM of calcein AM (AM = acetoxymethyl) for 30 min. Finally, the photocytotoxicity of proposed compounds were detected under fluorescent microscopy. Calcein AM (490 nm excitation and 515 nm emission filters) presented live cells in green color and PI (535 nm excitation and 615 nm emission filters) presented dead cells in red color.

3.4.4 Flow cytometry

MCF-7 cells 1×10^5 cells/well were seeded in a 6-well plate for 24 h. After that, the cells were treated with 5 μM of aza-BODIPY-mPEG for 0, 1, 4, 12, and 24 h. Then, the cells were washed with PBS buffer (pH 7.4) before being trypsinized to harvest the cells. The cells were centrifuged around 3000 rpm at 4 °C for 3 min and resuspended in an ice-cold PBS buffer (pH 7.4) for three times. Finally, 1×10^4 events were investigated following flow cytometry protocol using an Attune NxT Flow Cytometer (Thermo Fisher Scientific) using an excitation laser at 637 nm and emission filter 780/60 nm.

3.5 Chick Embryo and *In Ovo* Toxicity

3.5.1 Chick embryo chorioallantoic membrane (CAM) model

All of the results in chick embryo chorioallantoic membrane (CAM) model was studied by faculty of health and life sciences, Management and Science University, Shah Alam, Selangor, Malaysia. Fertilised Lohmann Brown chicken eggs were purchased from Hong Hing Sdn Bhd, Selangor, Malaysia, and sterilized with 70% ethanol. The eggs were incubated according the procedures described previously (Yadav, Sharma, and Kumar, 2020). On egg developmental day (EDD)-10, the viability of the embryos and vasculature of the CAM were visually inspected and randomly selected for the study.

3.5.2 Acute toxicity of NPs on chick embryo (*in ovo* toxicity)

Aza-BODIPY-A was dissolved in a cocktail of 50% cremophor EL and 50% EtOH, and diluted with saline to increase the volume of solution to 20 μ L for administration. **mPEG-COOH 5000** and **aza-BODIPY-mPEG** were dissolved and diluted in normal saline to the desired dose. On EDD-10, **Aza-BODIPY-A** at concentrations around 100-1000 μ g/mL was administered by using a microliter capillary syringe with a 33-gauge needle at the selected doses (n=3 per concentration at 20 μ L/embryo). The eggs were then sealed with parafilm and returned to the incubator for further observation. The mortality rate was recorded at 24 h. The chick embryo was considered alive in the case of no death observed at 48 h post-administration. The embryo was considered dead in the case of *in ovo* immobility and cloudy contents were observed.

3.6 *In Ovo* PTT Study

3.6.1 Anti-angiogenesis

On EDD-10, **aza-BODIPY-mPEG** at 10 μ g/embryo (500 μ g/mL), with an equivalent dose of **mPEG-COOH 5000** (8.9 μ g/embryo; 445 μ g/mL) and **aza-BODIPY-A** (1.1 μ g/embryo; 55 μ g/mL) were administered into the chick embryo at 20 μ L/embryo through intravenous injection (n=5 per group). After administration, a sterilized ring O was placed on the CAM for spot identification. After IV administration at 2 min, the targeted vessel was irradiated with 808 nm laser at 63 J/cm² (fluence rate

42 mW) for 60 s. The vasculature of CAM was photographed under a stereomicroscope at 10 min after-PTT process. The number of the blood vessel was calculated before and 10 min after-PTT process to determine the percentage of vasculature destruction.

3.6.2 Grafting of HCT116 tumor cells in CAM and photothermal therapy (PTT)

A human colorectal carcinoma cell (HCT116) in culture media was mixed with growth factor reduced Matrigel (8.9 mg/mL) in a ratio of 1:1. The mixtures were loaded on top of the CAM (EDD-10) at the volume of 25 μ L/embryo, with the density of 5×10^5 cells/embryo. Once implanted, the eggs were sealed with adhesive tape and returned to the incubator in the dark environment. On EDD-13, tumor mass grown on CAM was monitored, and randomly selected for the anti-cancer study. These **mPEG-COOH 5000**, **aza-BODIPY-A** and **aza-BODIPY-mPEG** (equivalent dose as described above) were intravenously administered into the chick embryo at 20 μ L/embryo (n=5 per group). At 2 min after administration, tumor tissue was irradiated under 808 nm laser at 63 J/cm² (fluence rate 42 mW) for 60 s. Tumor volume was measured by using calipers at 24 h, 48 h and 72 h after PTT process. The tumor volume (mm³) was calculated according to the equation of volume [(tumor width)² x tumor length/ 2].

3.6.3 Tumor tissue histopathology analysis

On EDD-17, the tumor tissues were monitored from the CAMs and immersed in 10% neutral buffered formalin followed by dehydration in ascending concentrations of ethanol (70%, 90% and 100%). The dehydrated tissues were cleared in xylene and also embedded in paraffin. The tissue blocks were cut into thickness section of about 5 μ m and stained with Hematoxylin and Eosin according to the histopathological examination. The 5 μ m thickness tissue sections were deparaffinized (remove the paraffin penetrated into the tissue) in xylene and rehydrated (replenishment of water lost through dehydration) in descending concentrations of alcohol in a sequential manner (100%, 90%, 80% and 70%; 2 min each). Thereafter, sections were stained in Harris's Haematoxylin for 1 min and washed with tap water; followed by immersion in 1% alcoholic Eosin-Y for 20 sec. After that, the sections were dehydrated in 70%, 80%, 90% and 100% of alcohol and cleared with xylene (2 min in each solution). Finally, the sections were mounted for tumor necrotic region identification (Böhm et al., 2019).

CHAPTER IV

RESULTS AND DISCUSSION

4.1 Synthesis and Characterization of aza-BODIPY NPs

The synthesis part consists of **aza-BODIPY-A** which was free dye and **aza-BODIPY-mPEG** which was nanoparticles. All compound structures were characterized by ^1H , ^{13}C , and ^{19}F NMR via the chemical shift (δ , ppm), resonance splitting, coupling constants (J), and a number of protons. Moreover, the **aza-BODIPY-A** was confirmed by its mass-to-charge ratio (m/z) to present the exact molecular weight by high-resolution Electrospray Ionization Time of Flight mass spectroscopy (high-resolution ESI-TOF-MS). And the **aza-BODIPY-mPEG** exact molecular weight was confirmed by MALDO-TOF spectrometer. The results were investigated to ensure the chemical structure of **aza-BODIPY-A** and **aza-BODIPY-mPEG** which showed in Figure 4.1-4.11.

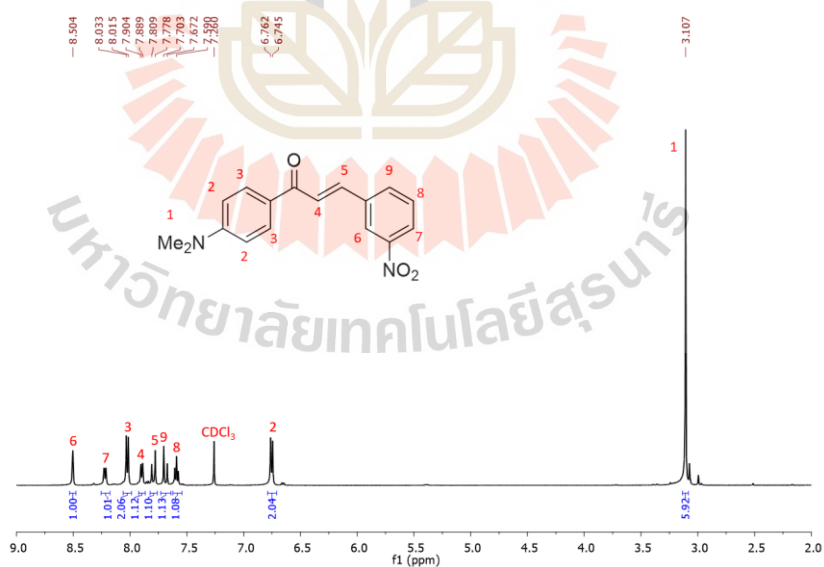
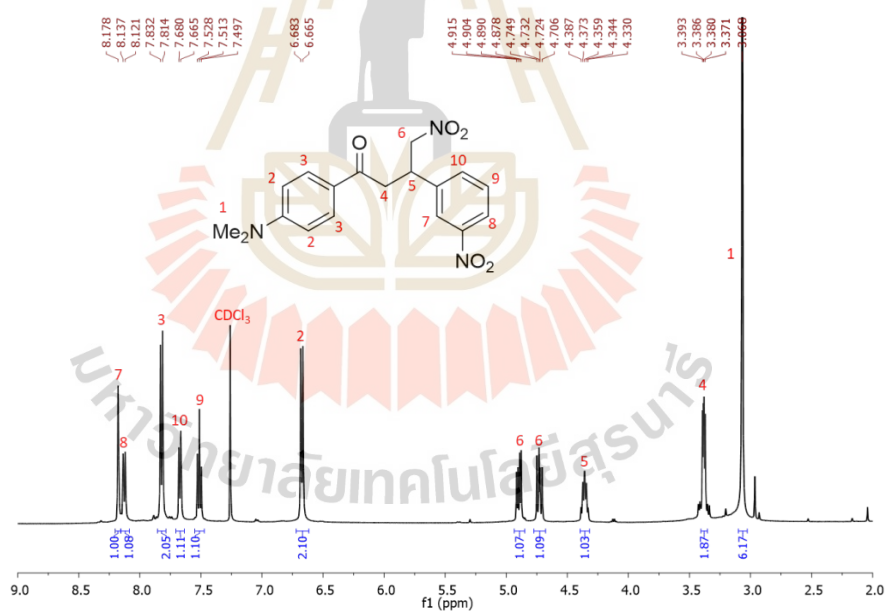
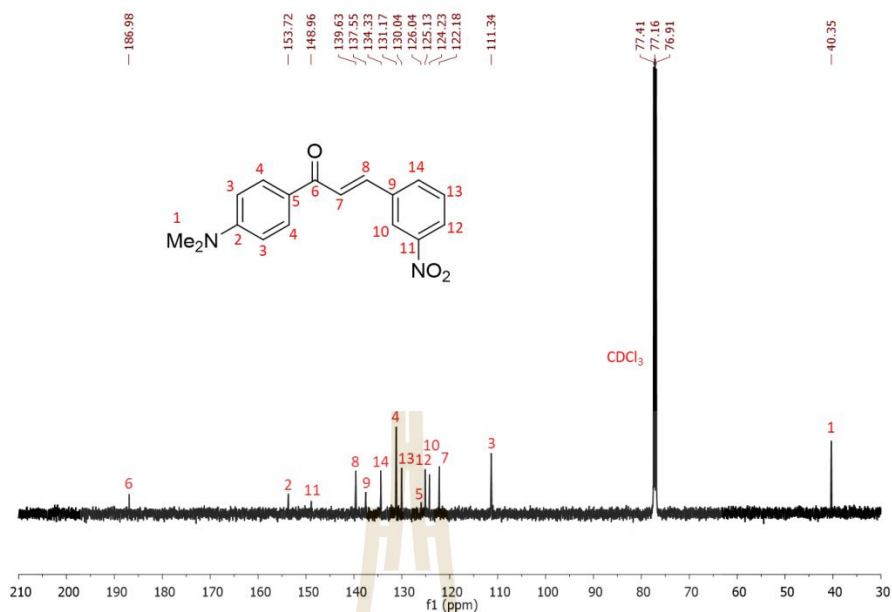
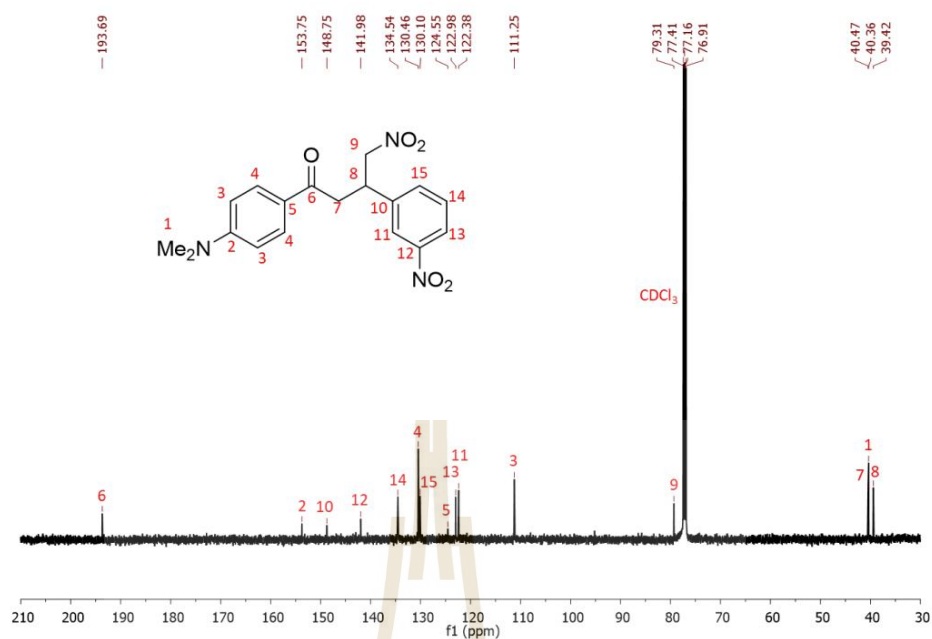
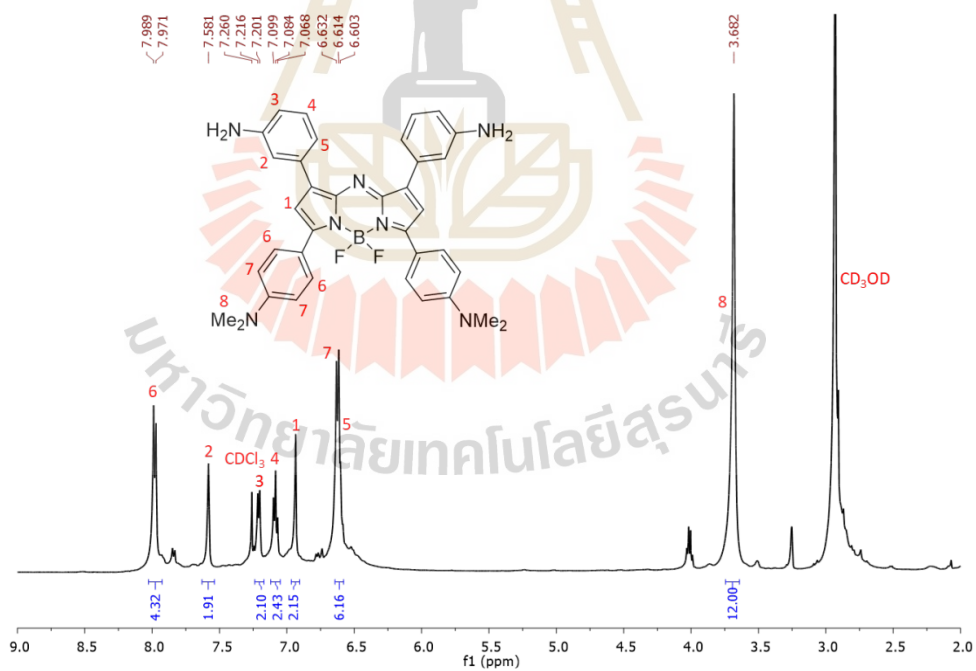
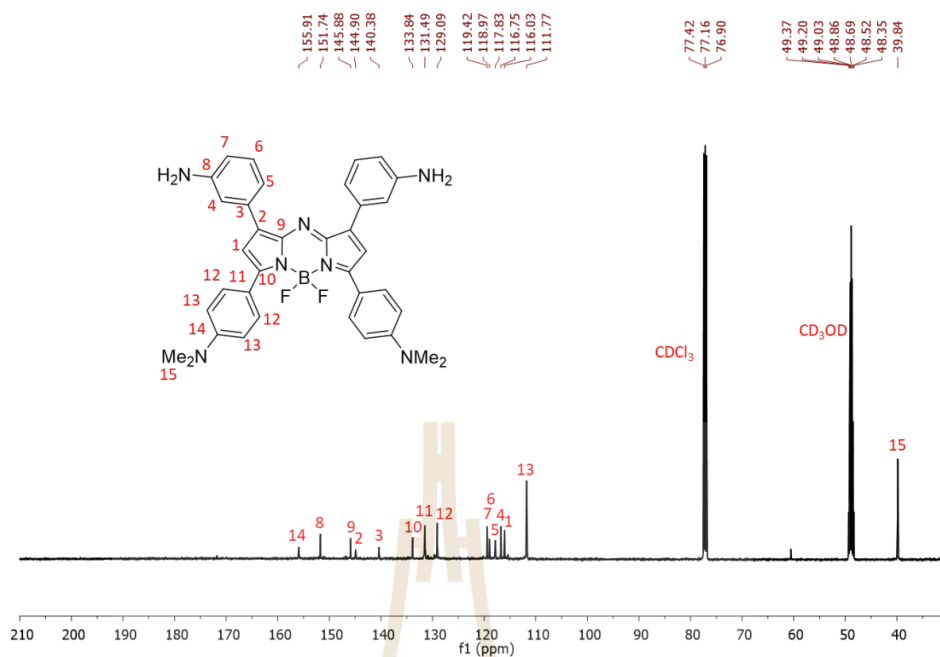
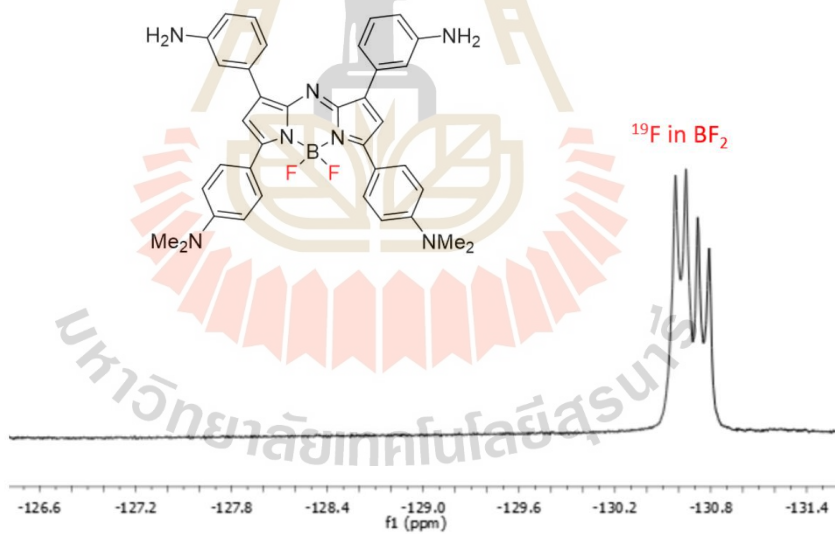


Figure 4.1 ^1H -NMR of compound 1.



Figure 4.4 ^{13}C -NMR of compound 2.Figure 4.5 ^1H -NMR of aza-BODIPY-A.

Figure 4.6 ¹³C-NMR of aza-BODIPY-A.Figure 4.7 ¹⁹F-NMR of aza-BODIPY-A.

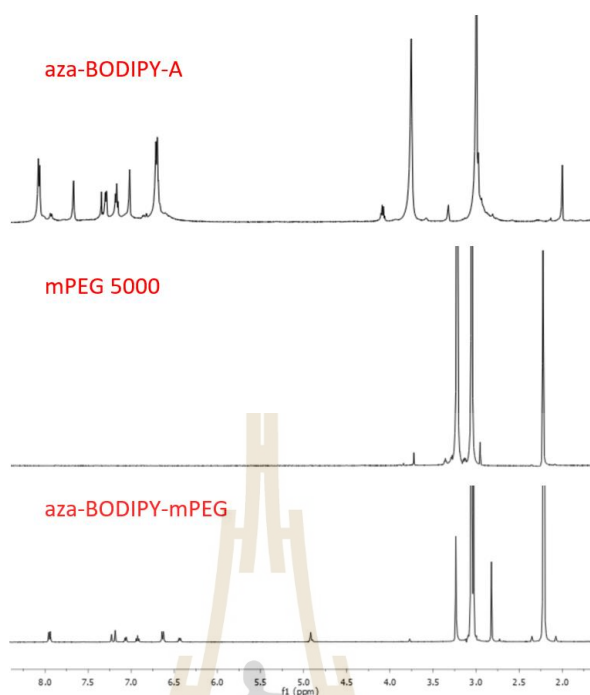


Figure 4.8 Comparison between $^1\text{H-NMR}$ of aza-BODIPY-A, mPEG and aza-BODIPY-mPEG.

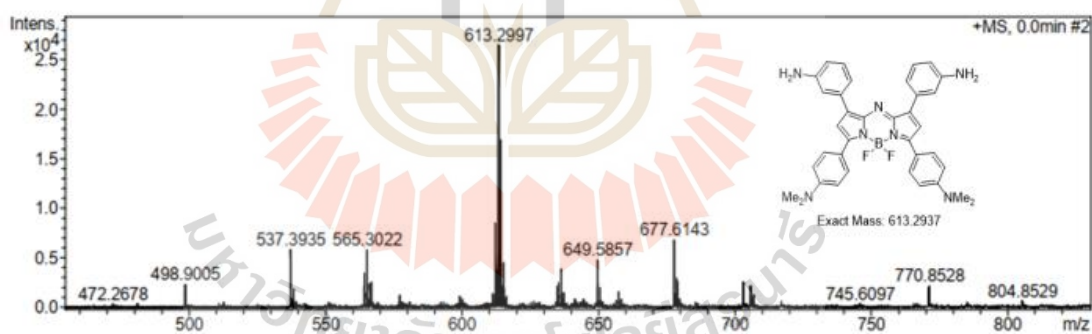


Figure 4.9 HRMS of aza-BODIPY-A.

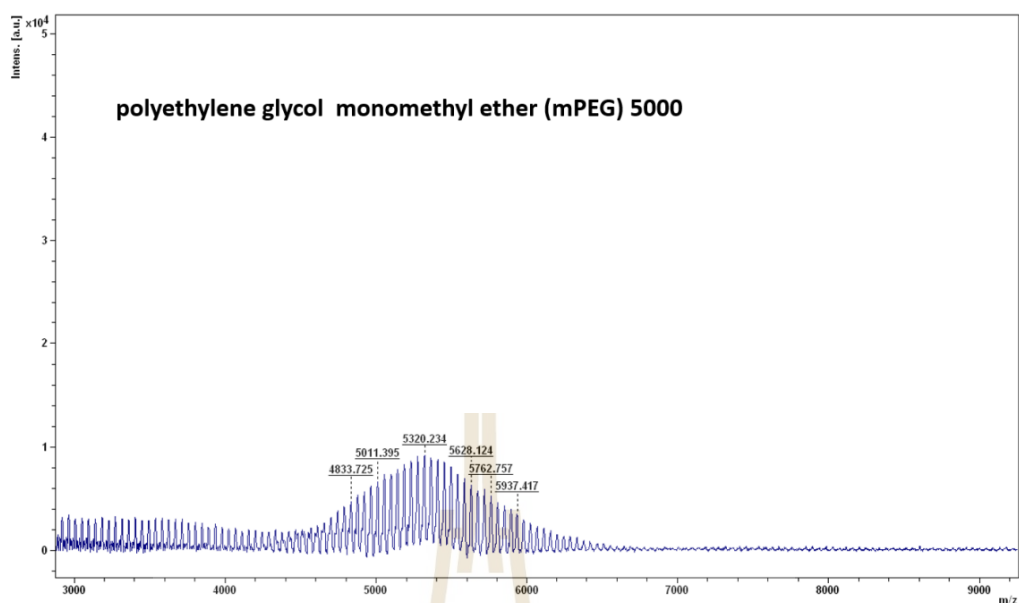


Figure 4.10 MALDI-TOF MS of mPEG-COOH.

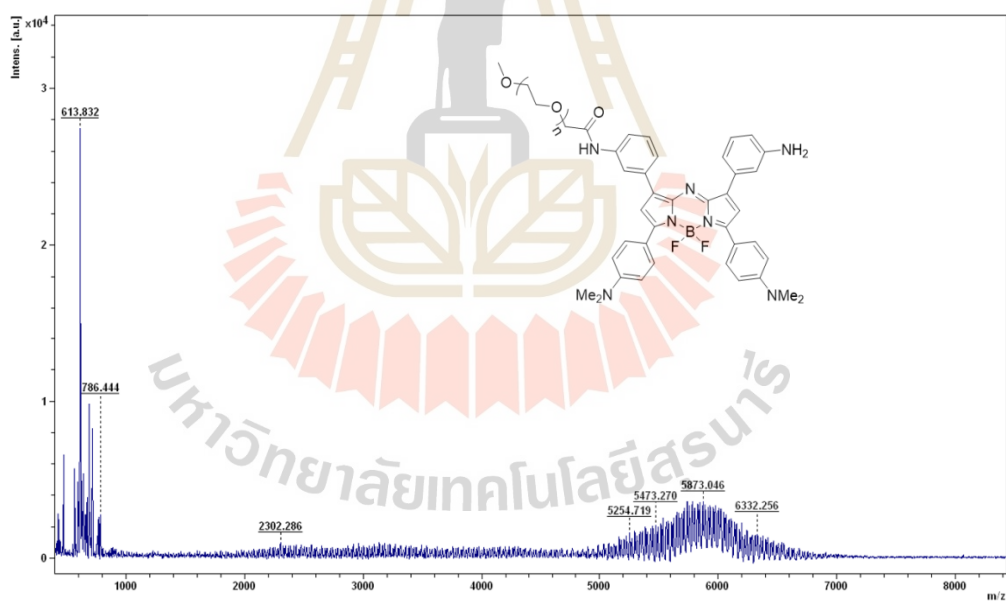


Figure 4.11 MALDI-TOF MS of aza-BODIPY-mPEG.

The preparation of **aza-BODIPY-mPEG** nanoparticle was synthesized by nano-conjugation via amide coupling between -NH_2 of aza-BODIPY-A with -COOH of mPEG-COOH molecular weight 5000 Da in a 1:1 ratio using EDC as a coupling reagent (Figure 4.12). After nano-conjugation, **aza-BODIPY-mPEG** nanoparticle was dissolved in DI

water and appeared in purple solution, which was different from aza-BODIPY-A free dye (Figure 4.13A).

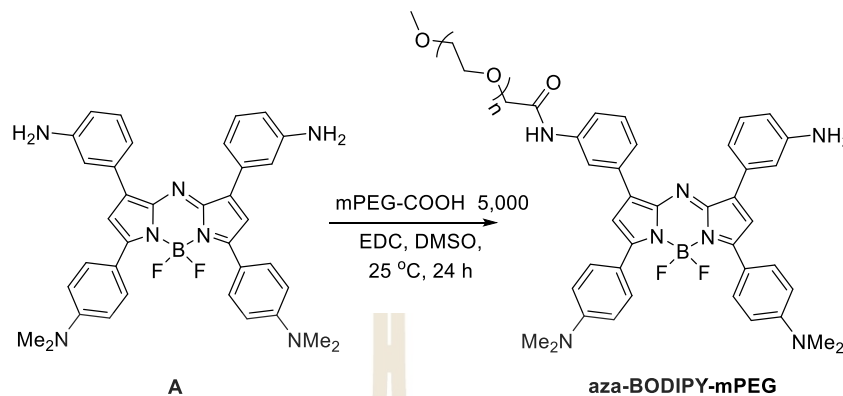


Figure 4.12 Synthesis of aza-BODIPY-mPEG.

Hydrodynamic (HD) size of aza-BODIPY-mPEG was characterized from dynamic light-scattering (DLS) technique. The HD size of aza-BODIPY-mPEG was 170 ± 1.09 nm (Figure 4.13B).

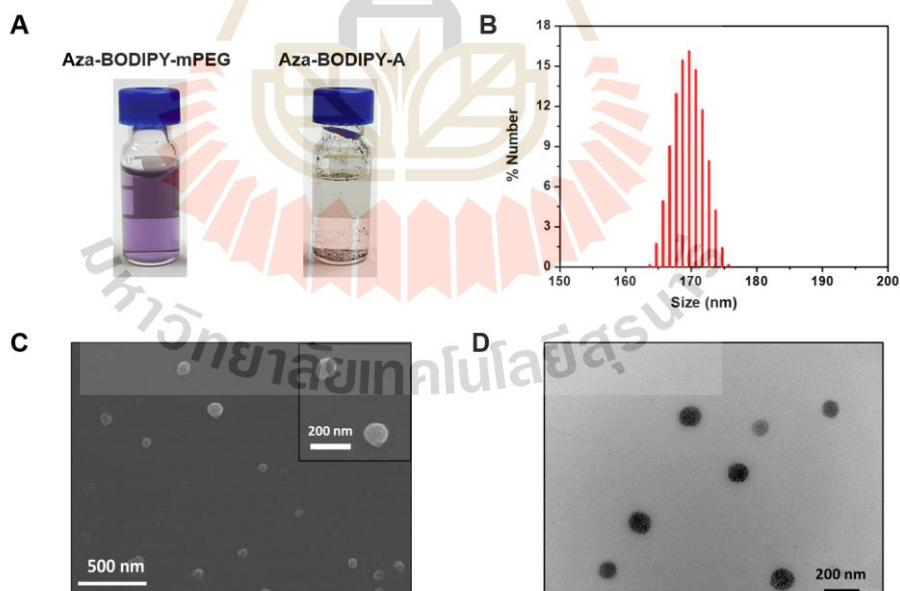


Figure 4.13 The aza-BODIPY-mPEG was well dispersed in water, as appeared in the purple solution which was different from the free dye (A) Photographs of aza-BODIPY-A and aza-BODIPY-mPEG in water. (B) hydrodynamic size distribution of aza-BODIPY-mPEG in water by DLS. (C) SEM and (D) TEM images of aza-BODIPY-mPEG.

The scanning electron microscopy (SEM) was used for spherical-shaped morphology of the **aza-BODIPY-mPEG** NPs (Figure 4.13C), while the transmission electron microscopy (TEM) demonstrated both isolated and agglomerate NPs (Figure 4.13D) with sizes ranging from 110 – 150 nm. The particle sizes obtained from electron microscopic techniques, were slightly smaller than those presented from DLS technique due to the hydrodynamic effect. The HD sizes of the NPs had similar in various solutions, including phosphate buffer saline (PBS), cell culture media (RPMI) and fetal bovine serum (FBS), Figure 4.14.

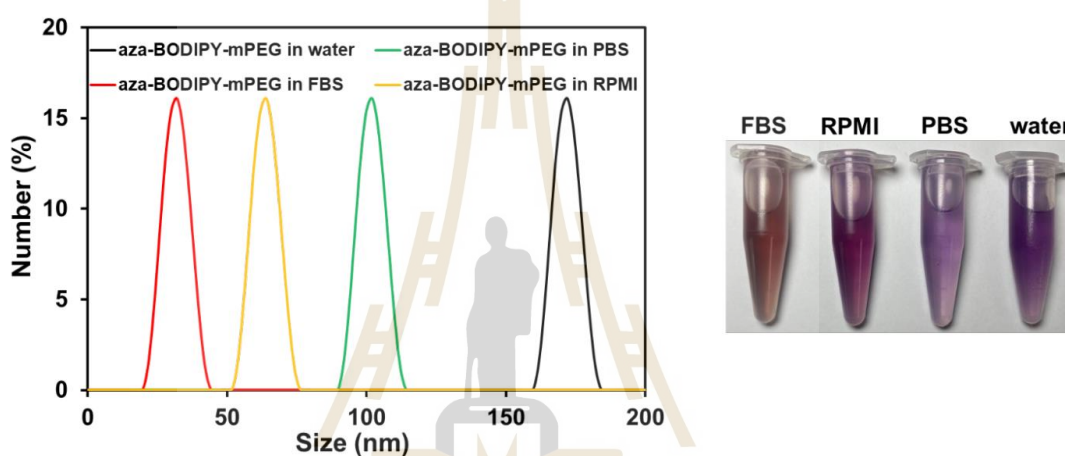


Figure 4.14 The hydrodynamic (HD) sizes of the NPs in various solutions including water, phosphate buffer saline (PBS), fetal bovine serum (FBS), and cell culture media (RPMI).

4.2 Photophysical properties of **aza-BODIPY-mPEG** NPs

The photophysical properties of **aza-BODIPY-mPEG** were expected to be similar to **aza-BODIPY-A**, which is its free dye form. Therefore, **aza-BODIPY-A** was investigated by a Vis-NIR spectrophotometer in various solvents to test its solubility soluble in water. As seen in Figure 4.15A and B, **aza-BODIPY-A** presented a broad absorption spectrum peaking at around 795, 799, and 827 nm in methanol, acetonitrile, and dimethyl sulfoxide respectively. Moreover, **aza-BODIPY-A** demonstrated maximum peak at 833 nm. Also, **aza-BODIPY-A** displayed flattened absorption spectra and low molar extinction coefficient (ϵ) in DI water, indicating poor water solubility. The fluorescence signal of **aza-BODIPY-mPEG** and **aza-BODIPY-A** were detected by DI

water and DMSO for radiative vibrational relaxation. As seen in Figure 4.15C, the fluorescent spectra of **aza-BODIPY-mPEG** and **aza-BODIPY-A** in various solvents displayed low emission peak suggesting possible non-radiative vibrational relaxation.

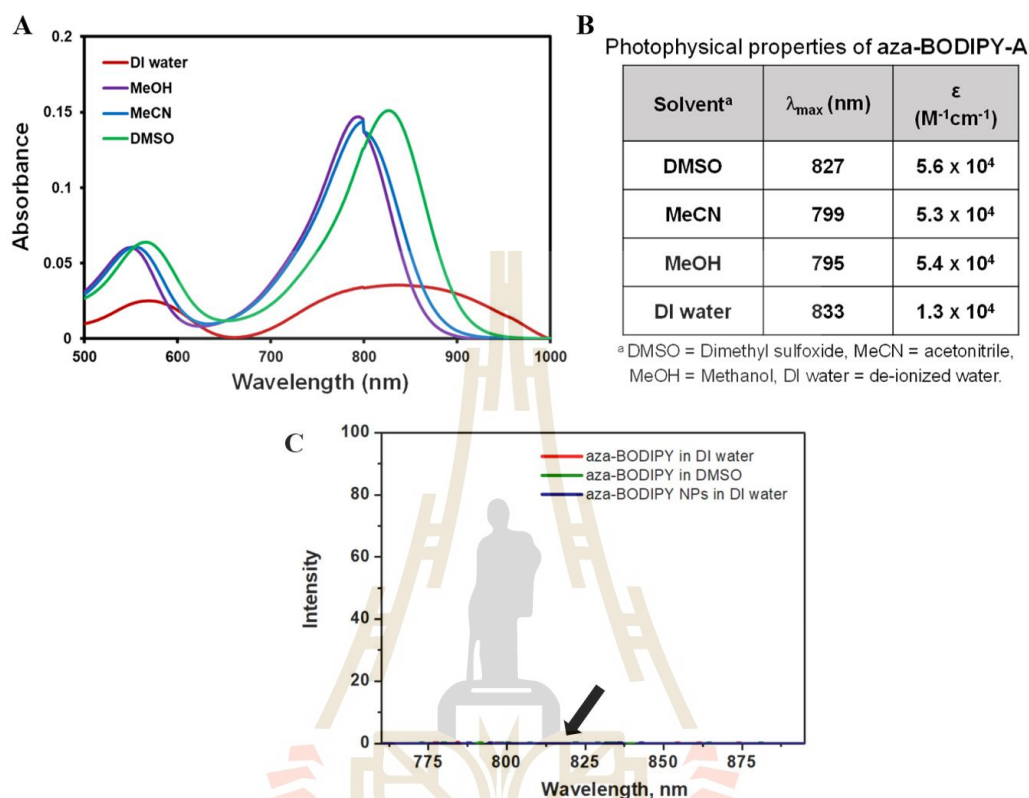


Figure 4.15 (A) Absorption spectra of **aza-BODIPY-A** in various solvents. (B) Photophysical Properties of **aza-BODIPY-A** ($3 \mu M$). (C) Fluorescence spectra of **aza-BODIPY-A** in DI water (red) and DMSO (green) compared to a fluorescent spectrum of **aza-BODIPY-mPEG** in DI water (blue).

After nano-conjugation synthetic, the Vis-NIR absorption of **aza-BODIPY-mPEG** NPs in DI water was similar to **aza-BODIPY-A** in DMSO, implying that the nanoparticle form could increase water solubility (Figure 4.16A). The NPs displayed NIR absorbance peaking at 842 nm with a 15 nm bathochromic shift compared with **aza-BODIPY-A** in DMSO, which was possibly attributed to the interaction of strong π - π stacking of **aza-BODIPY** molecules in the *J*-aggregation.(Y. Tian et al., 2022) This PTT phenomenon might occur because of the intramolecular charge transfer (ICT), the charge of electron-rich donor transferred to an electron-poor acceptor which belonged to the same

molecule, from electron-donating group, such as the NMe_2 and NH_2 groups attached to the aza-BODIPY core acting as the electron-accepting part (Rattanopas et al., 2020; Shi et al., 2020; Xu et al., 2021). In addition, there was no significant change in absorbance intensity as well as the heat signal of the NPs within 12 days, suggesting great photostability of **aza-BODIPY-mPEG** (Figure 4.16B).

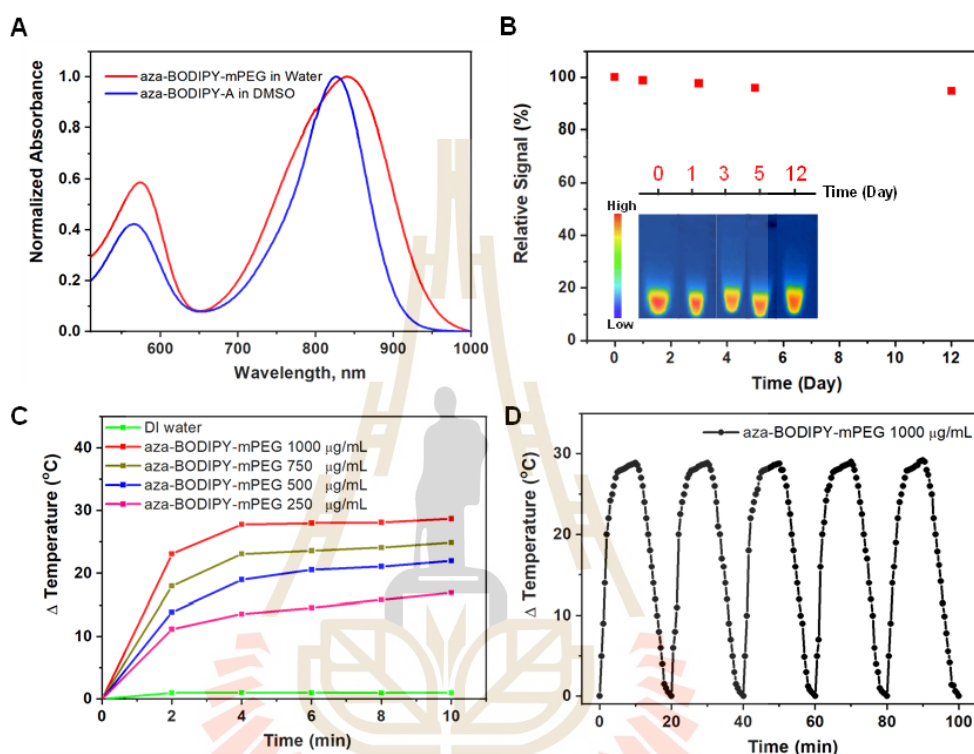


Figure 4.16 After conjugation, the vis-NIR absorption profile of azaBODIPY-mPEG NPs in DI water is similar to that of azaBODIPY-A in DMSO (A) Normalized absorbance of **aza-BODIPY-A** in DMSO and **aza-BODIPY-mPEG** in water. (B) Absorbance stability of **aza-BODIPY-mPEG** over time. Inset: Photograph of heat stability of the **aza-BODIPY-mPEG**. (C) Heating curves of **aza-BODIPY-mPEG** in aqueous solution with various concentrations at a power density of 0.7 W/cm^2 . (D) Photothermal stability test of **aza-BODIPY-mPEG** ($1000 \mu\text{g/mL}$) during five alternate heating-cooling cycles.

The disappearance of the fluorescent signal of **aza-BODIPY-mPEG** could be explained by the intramolecular PET process in the aza-BODIPY molecule (Rattanopas et al., 2020; Shi et al., 2020; Xu et al., 2021). The *N,N*-dimethylamino groups could assist the energy decay process at the excited state, which enhances the probability

of non-radiative transition that improved the photothermal conversion efficiency in the aza-BODIPY molecule. To evaluate the heat phenomenon from **aza-BODIPY-mPEG**, the NPs were dissolved in water and were irradiated with an 808 nm laser (0.7 W/ cm²) at various concentrations of 0, 250, 500, 750, and 1000 $\mu\text{g/mL}$. As shown in Figure 4.16C, the temperature of solution increases under photoirradiation correlated with the concentrations of the **aza-BODIPY-mPEG**. At 1000 $\mu\text{g/mL}$, the heat signal quickly increased around 23 °C after 120 s irradiation, and temperature alteration (ΔT) could eventually achieve 28 °C within 10 min, suggesting the significant photothermal effect of **aza-BODIPY-mPEG** could generate temperature signal. Additionally, the temperature of the NPs presents no abnormal change after irradiation at five cycles (OFF-ON laser, Figure 4.16D), indicating the excellent photothermal stability of **aza-BODIPY-mPEG**.

4.2.1 Photothermal conversion efficiency

The photothermal conversion efficiency of the aza-BODIPY-mPEG was calculated according to:

$$\eta = \frac{hs(T_{Max} - T_{Surr}) - Q_{Dis}}{I(1 - 10^{-A_{808}})} \quad (1)$$

Where h was the heat transfer coefficient, S was the surface area of the container and the value of hs was obtained from Eq.4 and Figure 4.17B. The maximum steady temperature (T_{max}) of the solution of the aza-BODIPY-mPEG was 58.9 °C and the environmental temperature (T_{Surr}) was 29 °C. So, the temperature change ($T_{Max} - T_{Surr}$) of the solution of the aza-BODIPY-mPEG was 29.5 °C. The laser power I was 0.5 W. The absorbance of the aza-BODIPY-mPEG at 808 nm A_{808} was 1.1145. Q_{Dis} expresses heat dissipated from the light absorbed by the solvent and container. To gain hS , a dimensionless parameter q was introduced as followed:

$$\theta = \frac{T - T_{Surr}}{T_{Max} - T_{Surr}} \quad (2)$$

A sample system time constant t_s could be calculated as Eq.3.

$$t = -\tau_s \ln(\theta) \quad (3)$$

According to Figure 17B, t_s was determined and calculated to be 279.44 s.

$$hs = \frac{m_D C_D}{\tau_s} \quad (4)$$

In addition, m was 0.5 g and C was 4.2 J/g·°C. Thus, according to Eq. 4, hS was deduced to be 0.015 mW/°C. Q_{Dis} expresses heat dissipated from the light absorbed by the quartz sample cell itself, and it was measured independently to be 0.0304 mW using a quartz cuvette cell containing pure water. Thus, substituting according to values of each parameter to Eq. 1, the 808 nm laser heat conversion efficiency (h) of the **aza-BODIPY-mPEG** could be calculated to be 41%.

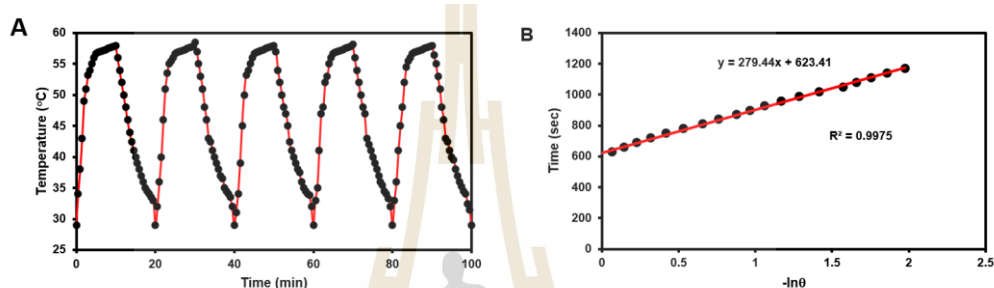


Figure 4.17 (a) Photothermal effect of the aqueous solution of the **aza-BODIPY-mPEG** (1 mg/mL) with the NIR laser (808 nm, 0.7 W/cm²) during five alternate heating-cooling cycles. (b) Linear time data versus $-\ln(\theta)$ obtained from the cooling period of (a).

4.3 Bio-applications of **aza-BODIPY** NPs

4.3.1 Live cell imaging

The cellular dose-dependent and time-dependent uptake of **aza-BODIPY-mPEG** was investigated in MCF-7 cells which is a human breast cancer cell line for a. The confocal images between **aza-BODIPY-mPEG** and MCF-7 cells revealed that the uptake of **aza-BODIPY-mPEG** by cells clearly increased within the first 12 h of incubation (Figure 4.18A). Following that, flow cytometry was investigated to analyze the probe's quantitative cell internalization. The results were detected by confocal imaging which the longer time exposure affected the higher the fluorescent signals (Figure 4.18B).

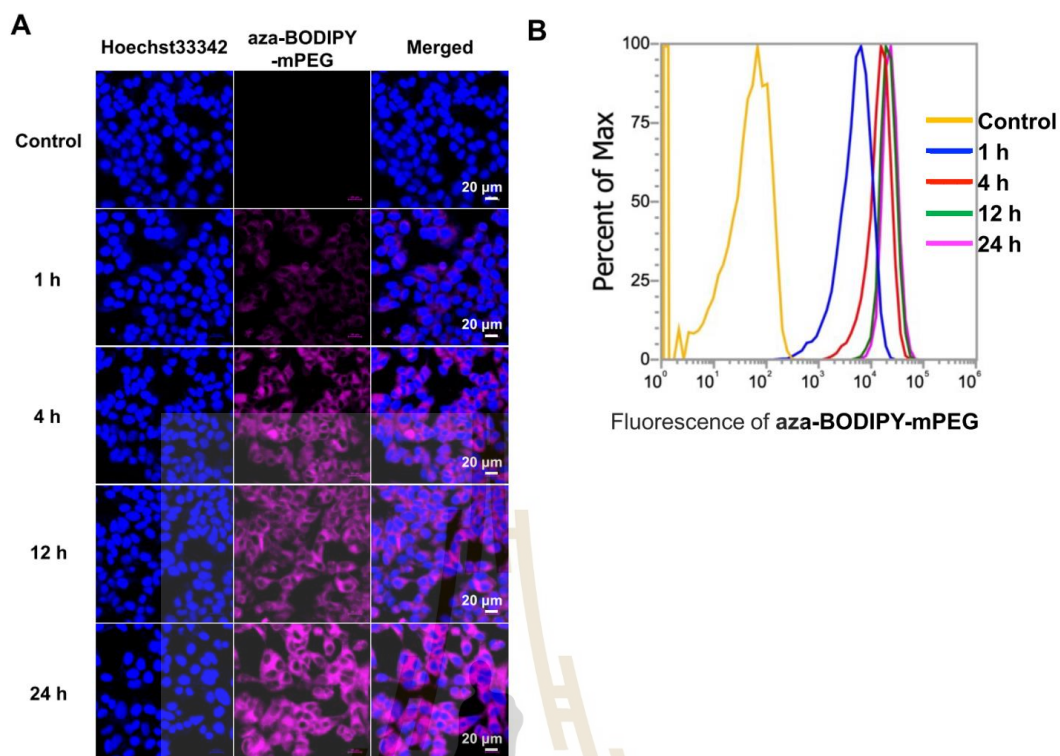


Figure 4.18 Cellular uptake of aza-BODIPY-mPEG. (A) Confocal images of MCF-7 treated with aza-BODIPY-mPEG (5 μM) for 0, 1, 4, 12, and 24 h. (B) Flow cytometry of MCF-7 cells incubated with 5 μM of aza-BODIPY-mPEG for 0, 1, 4, 12, and 24 h.

Moreover, the cellular uptake of azaBODIPY-mPEG was dose-dependent, in that the higher concentration of azaBODIPY-mPEG could produce a brighter signal in the cells (Figure 4.19A). Colocalization experiments were performed in MCF-7 cells to identify preferred organelles for aza-BODIPY-mPEG accumulation within cells. Aza-BODIPY-mPEG was managed within MCF-7 and colocalized to varying degrees with LysoTracker green (Pearson's R-value = 0.78), C6-NBD ceramide (golgi tracker, Pearson's R-value = 0.69), and MitoTracker Green (Pearson's R-value = 0.04). These results indicated that the probe was accumulated primarily in lysosomes and the golgi apparatus, but not in mitochondria (Figure 4.19B).

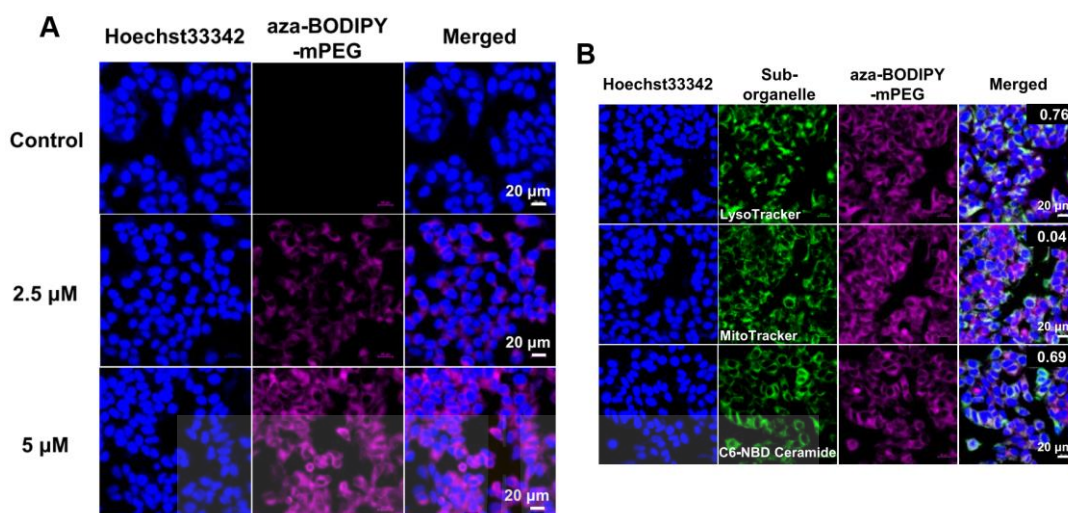


Figure 4.19 Cellular uptake of aza-BODIPY-mPEG (A) Confocal images of MCF-7 treated with aza-BODIPY-mPEG (2.5 and 5 μM) for 4 h. (B) Colocalization images of aza-BODIPY-mPEG (5 μM) at 4 h incubation with Hoechst 33342 (DNA fluorescent staining, blue) and organelle tracker: LysoTracker Green DND-26, MitoTracker Green FM, and C6-NBD Ceramide (golgi tracker, green). Scale bars = 20 μm .

4.3.2 Photocytotoxicity

The MTT (3-(4,5-dimethylthiazol-2-yl)-2,5-diphenyltetrazolium bromide) assay (Stockert, Horobin, Colombo, and Blázquez-Castro, 2018) was investigated to evaluate the photocytotoxicity of aza-BODIPY-mPEG on a human breast cancer cell line, MCF-7. In the case of non-laser irradiation, MCF-7 cells had a viability of over 90%, even at concentrations up to 20 μM , as shown in Figure 4.20A, suggesting low dark cytotoxicity and great biocompatibility of aza-BODIPY-mPEG. However, under 808 nm photoirradiation for 5 min (0.7 W/ cm^2), the cell survival decreased as the concentration of aza-BODIPY-mPEG increased, suggesting the cell survival was related with concentration of nanoparticle.

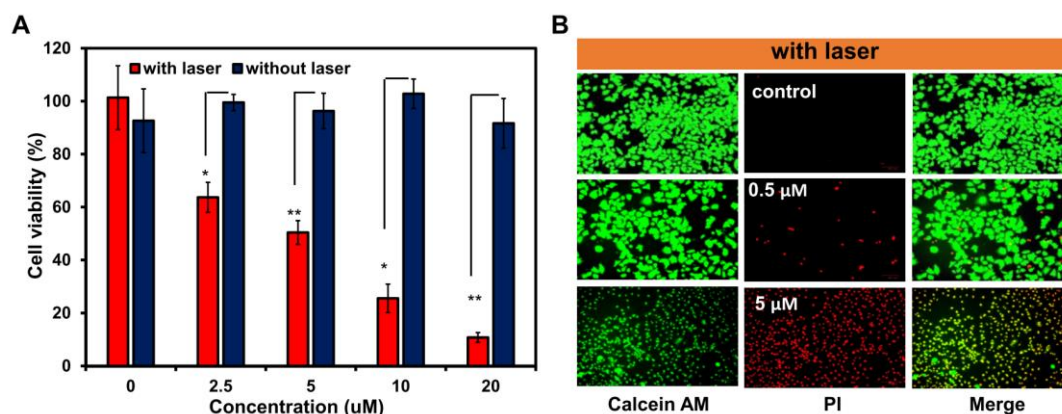


Figure 4.20 (A) The relative cell viability of MCF-7 under 808 nm photoirradiation at 5 min (0.7 W/ cm^2) after incubation with **aza-BODIPY-mPEG** (0–20 μM) for 6 h. Data are presented as means \pm SD ($n = 3$), * $P < 0.05$ or ** $P < 0.01$. (B) Fluorescent images of live/dead co-staining assay of MCF-7 cells after treatment with **aza-BODIPY-mPEG** (0.5 and 5 μM) for 6 h then irradiated at 5 min.

4.3.3 Live/Dead Staining

The live/dead cell assay was characterized to investigate the photocytotoxicity effect of the **aza-BODIPY-mPEG** NPs to live of cells before and after laser irradiation. Cells were treated with nonfluorescent calcein acetomethoxy (Calcein-AM), fluorescent dye could react intracellularly after esterase-dependent cellular trapping, indicated green fluorescence (under 488 nm excitation) after reaction with esterase within living cells, while propidium iodide (PI), a fluorescent intercalating agent could be using to stain cells and nucleic acids, could pass through the dead cell membrane to the nucleus, followed by integration with the nuclear DNA, subsequently producing red fluorescence ($\lambda_{\text{ex}} = 590 \text{ nm}$). MCF-7 cells treated with **aza-BODIPY-mPEG** and laser irradiation presented intense red fluorescence under confocal laser scanning microscopy (CLSM), whereas the control group which used for comparison showed no red fluorescence (Figure 4.20B). Furthermore, increasing the concentration of **aza-BODIPY-mPEG** could involve to increase red fluorescent signals which signifying a larger heat conversion for trigger cell death. As a result of their excellent biocompatibility and strong photocytotoxicity, **aza-BODIPY-mPEG** NPs could demonstrate to be promising and effective therapeutic agent for cancer phototherapy.

4.3.4 *In ovo* toxicity and anti-angiogenesis study

The toxicity of **aza-BODIPY-mPEG** was detected via intravenous route. The investigation was determined by the mortality of the chick embryo at 24 h post-administration. As shown in Figure 4.21A, **aza-BODIPY-mPEG** was found to be toxic to the chick embryos with LD₅₀ of 691 µg/mL and LD₅₀ of mPEG-COOH was 956 µg/mL. The result showed that **aza-BODIPY-A** exhibited no toxicity toward chick embryos. Hence, the non-toxic dose of **aza-BODIPY-mPEG** at 500 µg/mL was selected for anti-angiogenesis and anti-tumor studies.

For the anti-angiogenesis ability of **aza-BODIPY-mPEG** at 500 µg/mL after PTT study was investigated under chick embryo chorioallantoic membrane (CAM). There was no vasculature destruction observed in both saline-treated with control and mPEG-COOH-treated with samples at 445 µg/mL (equivalent concentration with **aza-BODIPY-mPEG** at 500 µg/mL). Both **aza-BODIPY-A** and **aza-BODIPY-mPEG** were showed vasculature destructive effects at 10 min after PTT study. **Aza-BODIPY-A**-treated CAM at 55 µg/mL (equivalent concentration with **aza-BODIPY-mPEG** at 500 µg/mL) showed thinner in the capillary compared to pre-PTT, and a large area of blood capillary disappearance was observed in **aza-BODIPY-mPEG**-treated CAM (Figure 4.21B). For quantification analysis, the number of blood vessels was counted for comparison between before and after PTT study at 10 min. Anti-angiogenic efficacy of **aza-BODIPY-mPEG** was high with vascular decreased to be $45 \pm 11\%$ after photoirradiation when compared with the **aza-BODIPY-A** which was $10.4 \pm 4.7\%$ destruction ($p= 0.008$). As for mPEG-COOH, it showed a very minor yet neglectable anti-angiogenic activity of $3.3 \pm 3.3\%$ whereas saline-treated with control groups did not show any vasculature destructive effects ($-1.5 \pm 1.5\%$) (Figure 4.21C).

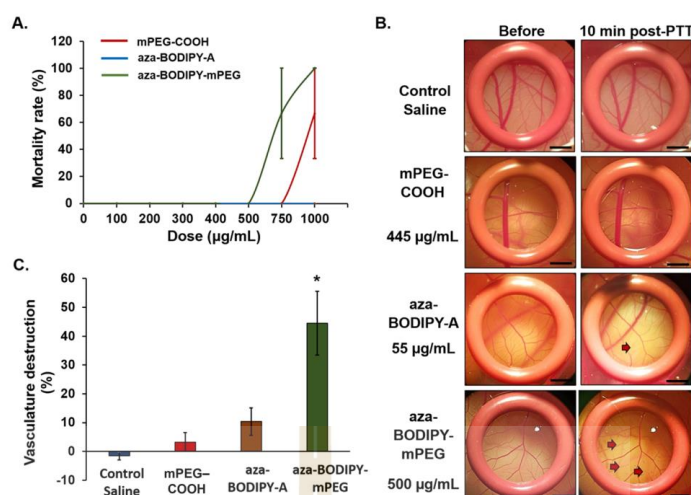


Figure 4.21 (A) Toxicity profile of mPEG-COOH, aza-BODIPY-A and aza-BODIPY-mPEG at concentration of 100-1000 $\mu\text{g/mL}$. Data are presented as means \pm SEM ($n = 3$). (B) The vasculature of chorioallantoic membrane within the ring O in pre- and post-PTT. The red arrow indicates the area of blood vessel destruction. Scale bar= 20 μm . Magnification 10x. The diagrams shown are representative of each group with similar observations. (C) The percentage of vasculature destruction of all groups at 10 min post-PTT. Data are presented as means \pm SEM ($n = 5$), * $p < 0.05$ based on One Way ANOVA.

The antitumor efficacy of aza-BODIPY-mPEG was evaluated *in ovo* using human colorectal carcinoma cell (HCT116) which was tumor xenograft in CAMs. The temperature of the tumor tissue was recorded before and during the irradiation by using 808 nm laser for 1 min. The CAM was treated by Aza-BODIPY-mPEG and the result showed that it could increase approximately 3-3.5 $^{\circ}\text{C}$ at 10 s of irradiation compared with before irradiation and maintained the temperature throughout 60 s of irradiation. CAM was treated Aza-BODIPY-A which it showed an increase in temperature (2-3 $^{\circ}\text{C}$), but lower than treated with aza-BODIPY-mPEG. Control saline and mPEG-COOH-treated CAM displayed similar temperatures throughout irradiation compared to after irradiation (Figure 12A). suggesting that the effectiveness of the aza-BODIPY-mPEG in delivering to the tumor tissue, and producing heat signal after irradiation.

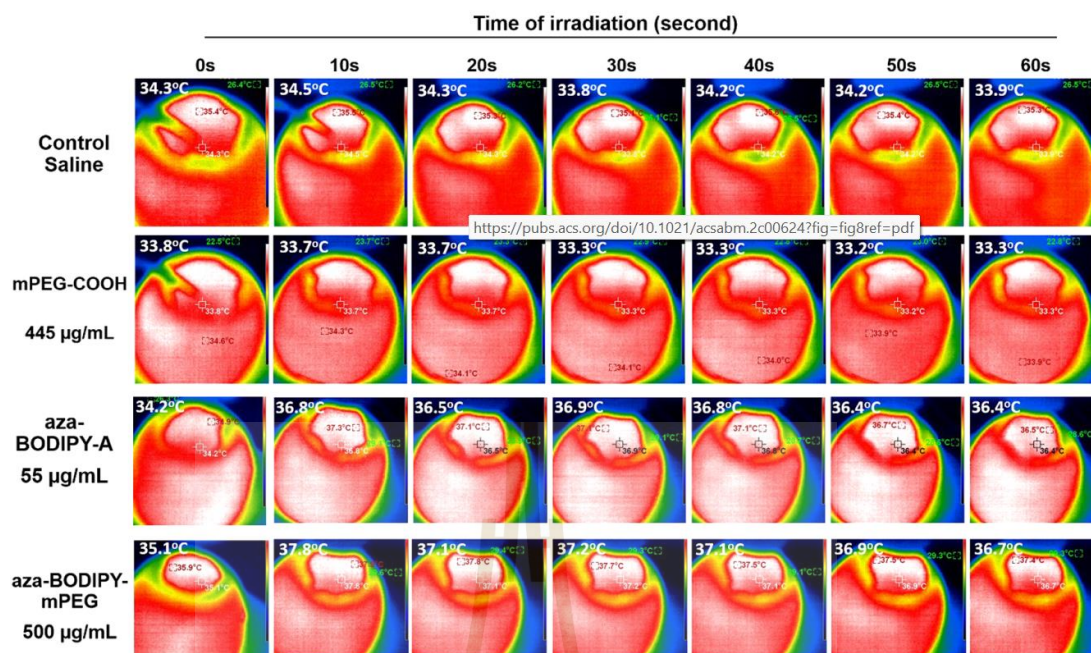


Figure 4.22 The temperature of the tumor tissue (white font) at different time points during irradiation.

The tumor tissue in the CAM after irradiation was observed daily, for 72 h. As shown in Figure 4.23A, saline and mPEG-COOH-treated with CAMs after PTT study showed comparable tumor volume with before the PTT study, up to 72 h. Comparatively, aza-BODIPY-A and aza-BODIPY-mPEG-treated with CAMs showed a reduction in the tumor volume, and darker in the color compared with before PTT study. For better comparison, the tumor growth curve was plotted across 3 days after PTT study. There was a slight increase yet comparable tumor volume in both saline- and mPEG-COOH-treated with CAMs. Aza-BODIPY-A- and aza-BODIPY-mPEG-treated CAMs showed 22.9% and 51.4% reduction in the tumor volume, respectively, at 72 h after PTT study ($p= 0.012$), suggesting aza-BODIPY-mPEG had better efficacy in inhibiting tumor growth (Figure 4.23B).

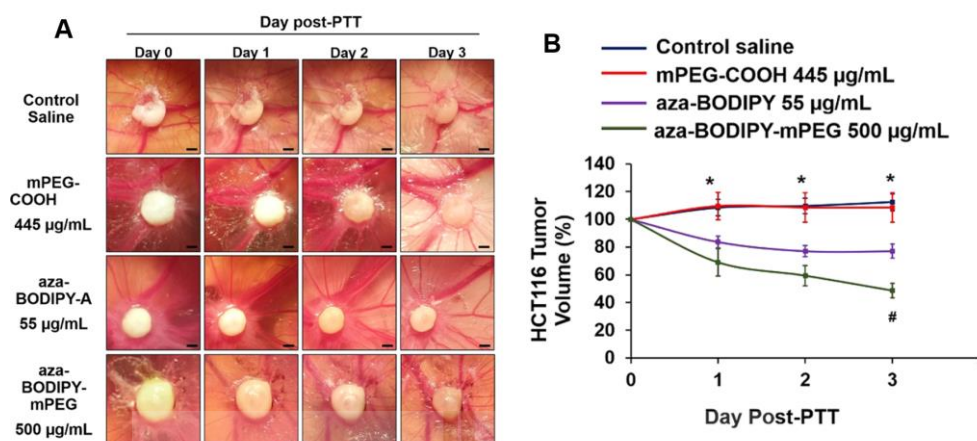


Figure 4.23 The antitumor efficacy of **aza-BODIPY-mPEG** was evaluated *in ovo* using human HCT116-implanted tumor xenograft in CAMs. (A) Human HCT116 tumor in CAM pre- (day 0) and post-PTT (day 1, 2, and 3). Scale bar = 20 µm. The diagrams shown were representative of each group, same egg for 3 days of observation. (B) Percentage of HCT116 tumor volume changes across 3 days of observation. Data was presented as means \pm SEM (n = 5), * p < 0.05, saline-treated control vs **aza-BODIPY-A** and **aza-BODIPY-mPEG**; # p < 0.05, **aza-BODIPY-A** vs **aza-BODIPY-mPEG** based on One Way ANOVA.

To confirm the decrease in tumor volume by the necrotic tumor tissue after PTT, tumor tissue was stained by hematoxylin and eosin (H&E). As shown in Figure 4.24A, when tumor tissue was treated by both the saline and mPEG-COOH, no noticeable cellular damage or inflammation to the tumor cells was observed. However, regional tumoral necrosis was observed in both groups treated with **aza-BODIPY-A** and **aza-BODIPY-mPEG**. In the case of tumor cells treated with **aza-BODIPY-mPEG**, the result showed more necrotic region. The tumor tissue was surrounded by blood vessels as followed by the presence of nucleated chick erythrocytes, which is indicated by the yellow arrows. In **aza-BODIPY-mPEG** which was treated with tumor tissue, there are many necrotic areas around the blood vessels, thus suggesting the successful delivery of the drug into the tumor microenvironment leading to cell death and necrosis after photoirradiation.

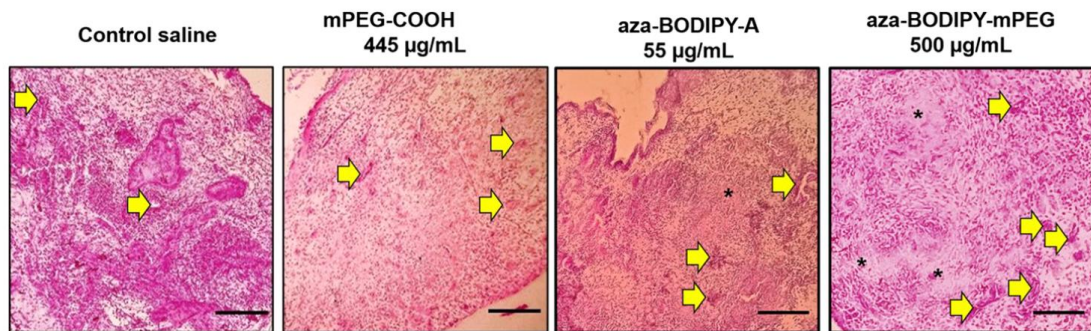


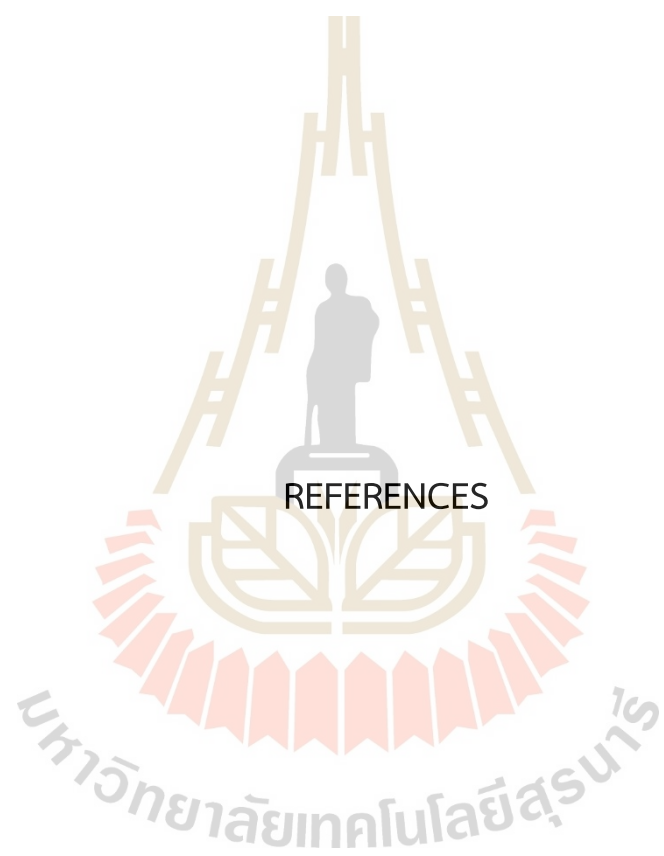
Figure 4.24 Hematoxylin and eosin-stained HCT116 tumor tissue at day 3 post-PTT. The yellow arrow indicates blood vessels, and the asterisk indicates the tumor necrotic area. Scale bar = 20 µm. Magnification 100x.



CHAPTER V

CONCLUSION

In conclusion, we synthesized **aza-BODIPY-A**, which had strong NIR absorption and photothermal conversion efficiency. Then, **aza-BODIPY-mPEG** was developed by conjugating the biocompatible polymer, mPEG-COOH, with aza-BODIPY via an amide bond that self-assembled to form **aza-BODIPY-mPEG** nanoparticles. The aza-BODIPY nano conjugation in this work and aza-BODIPY nano encapsulation that was tested *in vivo* from previous work were compared (Table S1). Our system was the only NPs formed by self-assembly of PEGylated aza-BODIPY. This was considered a convenient, scalable, and reproducible strategy in terms of material preparation. The conjugation formed self-assembly in water with hydrodynamic size at around 170 nm and the HD sizes presented smaller size when the NPs were dissolved in buffer or cell culture media. For photothermal study, when NPs were irradiated by 808 nm with a laser for 10 min, the NPs caused the solution temperature change (ΔT) of about +30 °C and this process could be repeated for at least five cycles without altering the photophysical properties of the NPs. In addition, for cancer treatment. **Aza-BODIPY-mPEG** exhibited photocytotoxicity towards breast cancer cells in a dose-dependent manner, and improved anti-angiogenic and antitumor activities, as compared to its parent **aza-BODIPY-A**. In conclusion, **aza-BODIPY-mPEG** appears to be a promising and effective therapeutic agent for cancer phototherapy.



REFERENCES

REFERENCES

- Auwah, S. G., and You, Y. (2012). Boron dipyrromethene (BODIPY)-based photosensitizers for photodynamic therapy. *RSC Advances*, 2(30), 11169-11183. doi:10.1039/C2RA21404K.
- Böhm, J., Muenzner, J. K., Caliskan, A., Ndreshkjana, B., Erlenbach-Wünsch, K., Merkel, S., Croner, R., Rau, T. T., Geppert, C. I., Hartmann, A., Roehe, A. V., and Schneider-Stock, R. (2019). Loss of enhancer of zeste homologue 2 (EZH2) at tumor invasion front is correlated with higher aggressiveness in colorectal cancer cells. *Journal of Cancer Research and Clinical Oncology*, 145(9), 2227-2240. doi:10.1007/s00432-019-02977-1.
- Bray, F., Ferlay, J., Soerjomataram, I., Siegel, R. L., Torre, L. A., and Jemal, A. (2018). Global cancer statistics 2018: GLOBOCAN estimates of incidence and mortality worldwide for 36 cancers in 185 countries. *CA Cancer J Clin*, 68(6), 394-424. doi:10.3322/caac.21492
- Carneiro, B. A., and El-Deiry, W. S. (2020). Targeting apoptosis in cancer therapy. *Nature Reviews Clinical Oncology*, 17(7), 395-417. doi:10.1038/s41571-020-0341-y.
- Chansaenpak, K., Tanjindaprateep, S., Chaicharoenaudomrung, N., Weeranantanapan, O., Noisa, P., and Kamkaew, A. (2018). Aza-BODIPY based polymeric nanoparticles for cancer cell imaging. *RSC Advances*, 8(69), 39248-39255. doi:10.1039/C8RA08145J.
- Chen, D., Zhang, J., Tang, Y., Huang, X., Shao, J., Si, W., Ji, J., Zang, Q., Huang, W., and Dong, X. (2018). A tumor-mitochondria dual targeted aza-BODIPY-based nanotheranostic agent for multimodal imaging-guided phototherapy. *Journal of Materials Chemistry B*, 6(27), 4522-4530. doi:10.1039/C8TB01347K.
- Chen, D., Zhong, Z., Ma, Q., Shao, J., Huang, W., and Dong, X. (2020). Aza-BODIPY-Based Nanomedicines in Cancer Phototheranostics. *ACS Applied Materials and Interfaces*, 12(24), 26914-26925. doi:10.1021/acsami.0c05021.

- Cheng, M. H. Y., Maruani, A., Savoie, H., Chudasama, V., and Boyle, R. W. (2018). Synthesis of a novel HER2 targeted aza-BODIPY-antibody conjugate: synthesis, photophysical characterisation and in vitro evaluation. *Organic and Biomolecular Chemistry*, *16*(7), 1144-1149. doi:10.1039/C7OB02957H.
- Cohen, S., Yoshioka, T., Lucarelli, M., Hwang, L. H., and Langer, R. (1991). Controlled Delivery Systems for Proteins Based on Poly(Lactic/Glycolic Acid) Microspheres. *Pharmaceutical Research*, *8*(6), 713-720. doi:10.1023/A:1015841715384.
- Cortezon-Tamarit, F., Ge, H., Mirabello, V., Theobald, M. B. M., Calatayud, D. G., and Pascu, S. I. (2017). Chapter Eight - Carbon Nanotubes and Related Nanohybrids Incorporating Inorganic Transition Metal Compounds and Radioactive Species as Synthetic Scaffolds for Nanomedicine Design. In K. K.-W. Lo (Ed.), *Inorganic and Organometallic Transition Metal Complexes with Biological Molecules and Living Cells* (pp. 245-327): Academic Press.
- Curtin, N. J. (2012). DNA repair dysregulation from cancer driver to therapeutic target. *Nature Reviews Cancer*, *12*(12), 801-817. doi:10.1038/nrc3399.
- Fernandez-Fernandez, A., Manchanda, R., Carvajal, D. A., Lei, T., Srinivasan, S., and McGoron, A. J. (2014). Covalent IR820-PEG-diamine nanoconjugates for theranostic applications in cancer. *Int J Nanomedicine*, *9*, 4631-4648. doi:10.2147/ijn.S69550.
- Ferrari, M. (2005). Cancer nanotechnology: opportunities and challenges. *Nature Reviews Cancer*, *5*(3), 161-171. doi:10.1038/nrc1566.
- Gajendiran, M., Jo, H., Kim, K., and Balasubramanian, S. (2019). Green synthesis of multifunctional PEG-carboxylate π back-bonded gold nanoconjugates for breast cancer treatment. *Int J Nanomedicine*, *14*, 819-834. doi:10.2147/ijn.S190946.
- Gao, D., Zhang, B., Liu, Y., Hu, D., Sheng, Z., Zhang, X., and Yuan, Z. (2019). Molecular Engineering of Near-Infrared Light-Responsive BODIPY-Based Nanoparticles with Enhanced Photothermal and Photoacoustic Efficiencies for Cancer Theranostics. *Theranostics*, *9*(18), 5315-5331. doi:10.7150/thno.34418.

- Hu, L., Wang, P., Zhao, M., Liu, L., Zhou, L., Li, B., Albaqami, F. H., El-Toni, A. M., Li, X., Xie, Y., Sun, X., and Zhang, F. (2018). Near-infrared rechargeable “optical battery” implant for irradiation-free photodynamic therapy. *Biomaterials*, *163*, 154-162. doi:<https://doi.org/10.1016/j.biomaterials.2018.02.029>.
- Hu, W., Ma, H., Hou, B., Zhao, H., Ji, Y., Jiang, R., Hu, X., Lu, X., Zhang, L., Tang, Y., Fan, Q., and Huang, W. (2016). Engineering Lysosome-Targeting BODIPY Nanoparticles for Photoacoustic Imaging and Photodynamic Therapy under Near-Infrared Light. *ACS Applied Materials and Interfaces*, *8*(19), 12039-12047. doi:[10.1021/acsami.6b02721](https://doi.org/10.1021/acsami.6b02721).
- Iyer, A. K., Khaled, G., Fang, J., and Maeda, H. (2006). Exploiting the enhanced permeability and retention effect for tumor targeting. *Drug Discovery Today*, *11*(17), 812-818. doi:<https://doi.org/10.1016/j.drudis.2006.07.005>.
- Jiang, X.-D., Xi, D., Sun, C.-L., Guan, J., He, M., and Xiao, L.-J. (2015). Synthesis of a pyrene-fused aza-BODIPY as a near-infrared dye having the absorption maximum at 746nm. *Tetrahedron Letters*, *56*(34), 4868-4870. doi:[10.1016/j.tetlet.2015.06.053](https://doi.org/10.1016/j.tetlet.2015.06.053).
- Kamaly, N., Yameen, B., Wu, J., and Farokhzad, O. C. (2016). Degradable Controlled-Release Polymers and Polymeric Nanoparticles: Mechanisms of Controlling Drug Release. *Chemical Reviews*, *116*(4), 2602-2663. doi:[10.1021/acs.chemrev.5b00346](https://doi.org/10.1021/acs.chemrev.5b00346).
- Kang, H., Rho, S., Stiles, W. R., Hu, S., Baek, Y., Hwang, D. W., Kachiwaki, S., Kim, M. S., and Choi, H. S. (2020). Size-Dependent EPR Effect of Polymeric Nanoparticles on Tumor Targeting. *Advanced Healthcare Materials*, *9*(1), 1901223. doi:[10.1002/adhm.201901223](https://doi.org/10.1002/adhm.201901223).
- Li, S., Zou, Q., Li, Y., Yuan, C., Xing, R., and Yan, X. (2018). Smart Peptide-Based Supramolecular Photodynamic Metallo-Nanodrugs Designed by Multicomponent Coordination Self-Assembly. *Journal of the American Chemical Society*, *140*(34), 10794-10802. doi:[10.1021/jacs.8b04912](https://doi.org/10.1021/jacs.8b04912).

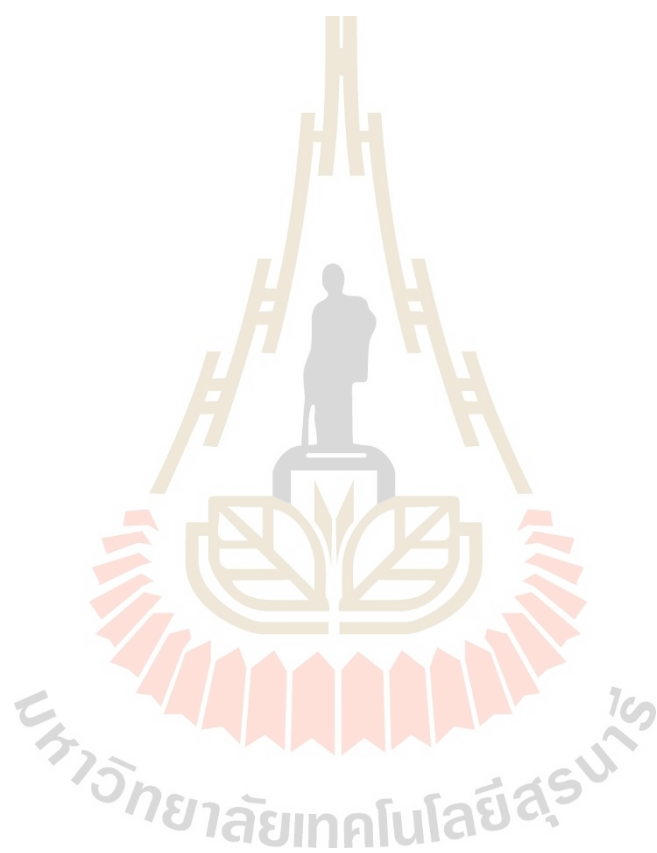
- Li, X., Kim, C. y., Lee, S., Lee, D., Chung, H.-M., Kim, G., Heo, S. H., Kim, C., Hong, K. S., and Yoon, J. (2017). Nanostructured Phthalocyanine Assemblies with Protein-Driven Switchable Photoactivities for Biophotonic Imaging and Therapy. *Journal of the American Chemical Society*, 139(31), 10880-10886. doi:10.1021/jacs.7b05916.
- Liang, C., Xu, L., Song, G., and Liu, Z. (2016). Emerging nanomedicine approaches fighting tumor metastasis: animal models, metastasis-targeted drug delivery, phototherapy, and immunotherapy. *Chemical Society Reviews*, 45(22), 6250-6269. doi:10.1039/C6CS00458J.
- Liu, Y., Shen, G., Zhao, L., Zou, Q., Jiao, T., and Yan, X. (2019). Robust Photothermal Nanodrugs Based on Covalent Assembly of Nonpigmented Biomolecules for Antitumor Therapy. *ACS Applied Materials & Interfaces*, 11(45), 41898-41905. doi:10.1021/acsami.9b13966.
- Liu, Y., Sun, D., Fan, Q., Ma, Q., Dong, Z., Tao, W., Tao, H., Liu, Z., and Wang, C. (2020). The enhanced permeability and retention effect based nanomedicine at the site of injury. *Nano Research*, 13(2), 564-569. doi:10.1007/s12274-020-2655-6
- Ma, Y., Huang, J., Song, S., Chen, H., and Zhang, Z. (2016). Cancer-Targeted Nanotheranostics: Recent Advances and Perspectives. *Small*, 12. doi:10.1002/sml.201600635.
- Maeda, H., Bharate, G. Y., and Daruwalla, J. (2009). Polymeric drugs for efficient tumortargeted drug delivery based on EPR-effect. *European Journal of Pharmaceutics and Biopharmaceutics*, 71(3), 409-419. doi:10.1016/j.ejpb.2008.11.010.
- Maeda, H., Fang, J., Inutsuka, T., and Kitamoto, Y. (2003). Vascular permeability enhancement in solid tumor: Various factors, mechanisms involved and its implications. *International immunopharmacology*, 3, 319-328. doi:10.1016/S1567-5769(02)00271-0.
- Ni, Y., Kannadorai, R. K., Peng, J., Yu, S. W. K., Chang, Y.-T., and Wu, J. (2016). Naphthalenefused BODIPY near-infrared dye as a stable contrast agent for in vivo photoacoustic imaging. *Chemical Communications*, 52(77), 11504-11507. doi:10.1039/C6CC05126J.

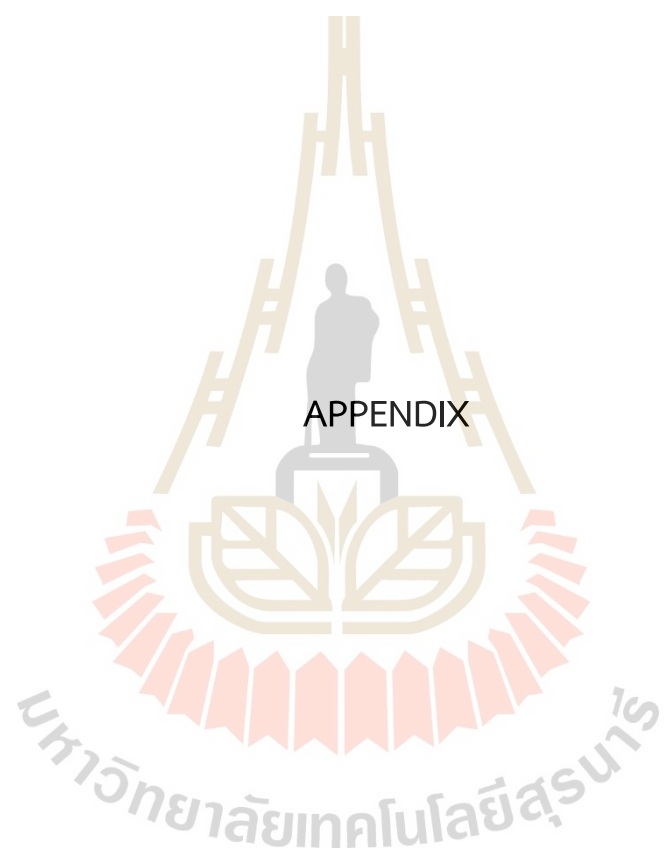
- Niu, S. L., Ulrich, G., Ziesel, R., Kiss, A., Renard, P.-Y., and Romieu, A. (2009). Water-Soluble BODIPY Derivatives. *Organic Letters*, 11(10), 2049-2052. doi:10.1021/ol900302n.
- Perry, J. L., Reuter, K. G., Luft, J. C., Pecot, C. V., Zamboni, W., and DeSimone, J. M. (2017). Mediating Passive Tumor Accumulation through Particle Size, Tumor Type, and Location. *Nano Letters*, 17(5), 2879-2886. doi:10.1021/acs.nanolett.7b00021.
- Rattanopas, S., Chansaenpak, K., Siwawannapong, K., Ngamchuea, K., Wet-osot, S., Treekoon, J., Pewklang, T., Jinaphon, T., Sagarik, K., Lai, R. Y., Cheng, L., and Kamkaew, A. (2020). Synthesis and Characterization of Push-Pull Aza-BODIPY Dyes Towards Application in NIR-II Photothermal Therapy. *ChemPhotoChem*, 4(11), 5304-5311. doi:https://doi.org/10.1002/cptc.202000164.
- Ribas, A., and Wolchok, J. D. (2018). Cancer immunotherapy using checkpoint blockade. *Science (New York, N.Y.)*, 359(6382), 1350-1355. doi:10.1126/science.aar4060.
- Shi, Z., Han, X., Hu, W., Bai, H., Peng, B., Ji, L., Fan, Q., Li, L., and Huang, W. (2020). Bioapplications of small molecule Aza-BODIPY: from rational structural design to *in vivo* investigations. *Chemical Society Reviews*, 49(21), 7533-7567. doi:10.1039/D0CS00234H.
- Siwawannapong, K., Zhang, R., Lei, H., Jin, Q., Tang, W., Dong, Z., Lai, R. Y., Liu, Z., Kamkaew, A., and Cheng, L. (2020). Ultra-small Pyropheophorbide-a Nanodots for Near-infrared Fluorescence/Photoacoustic Imaging-guided Photodynamic Therapy. *Theranostics*, 10(1), 62-73. doi:10.7150/thno.35735.
- Stockert, J. C., Horobin, R. W., Colombo, L. L., and Blázquez-Castro, A. (2018). Tetrazolium salts and formazan products in Cell Biology: Viability assessment, fluorescence imaging, and labeling perspectives. *Acta Histochemica*, 120(3), 159-167. doi:https://doi.org/10.1016/j.acthis.2018.02.005.
- Tang, Q., Si, W., Huang, C., Ding, K., Huang, W., Chen, P., Zhang, Q., and Dong, X. (2017). An aza-BODIPY photosensitizer for photoacoustic and photothermal imaging guided dual modal cancer phototherapy. *Journal of Materials Chemistry B*, 5(8), 1566- 1573. doi:10.1039/C6TB02979E.

- Tang, Q., Xiao, W., Huang, C., Si, W., Shao, J., Huang, W., Chen, P., Zhang, Q., and Dong, X. (2017). pH-Triggered and Enhanced Simultaneous Photodynamic and Photothermal Therapy Guided by Photoacoustic and Photothermal Imaging. *Chemistry of Materials*, 29(12), 5216-5224. doi:10.1021/acs.chemmater.7b01075.
- Tang, Y., Xue, L., Yu, Q., Chen, D., Cheng, Z., Wang, W., Shao, J., and Dong, X. (2019). Smart Aza-BODIPY Photosensitizer for Tumor Microenvironment-Enhanced Cancer Phototherapy. *ACS Applied Bio Materials*, 2(12), 5888-5897. doi:10.1021/acsabm.9b00836.
- Tian, J., Chen, J., Ge, C., Liu, X., He, J., Ni, P., and Pan, Y. (2016). Synthesis of PEGylated Ferrocene Nanoconjugates as the Radiosensitizer of Cancer Cells. *Bioconjugate Chemistry*, 27(6), 1518-1524. doi:10.1021/acs.bioconjchem.6b00168
- Tian, Y., Yin, D., Cheng, Q., Dang, H., Teng, C., and Yan, L. (2022). Supramolecular J-aggregates of aza-BODIPY by steric and π - π interactions for NIR-II phototheranostics. *Journal of Materials Chemistry B*, 10(10), 1650-1662. doi:10.1039/D1TB02820K.
- Wirthl, B., Kremheller, J., Schrefler, B. A., and Wall, W. A. (2020). Extension of a multiphase tumour growth model to study nanoparticle delivery to solid tumours. *PLoS ONE*, 15(2), e0228443. doi:10.1371/journal.pone.0228443.
- Wong, A. D., Ye, M., Ulmschneider, M. B., and Searson, P. C. (2015). Quantitative Analysis of the Enhanced Permeation and Retention (EPR) Effect. *PLoS ONE*, 10(5), e0123461. doi:10.1371/journal.pone.0123461.
- Xing, R., Zou, Q., Yuan, C., Zhao, L., Chang, R., and Yan, X. (2019). Self-Assembling Endogenous Biliverdin as a Versatile Near-Infrared Photothermal Nanoagent for Cancer Theranostics. *Advanced Materials*, 31, 1900822. doi:10.1002/adma.201900822.
- Xu, Y., Wang, S., Chen, Z., Hu, R., Li, S., Zhao, Y., Liu, L., and Qu, J. (2021). Highly stable organic photothermal agent based on near-infrared-II fluorophores for tumor treatment. *Journal of Nanobiotechnology*, 19(1), 37. doi:10.1186/s12951-021-00782-y.

Yadav, S., Sharma, A. K., and Kumar, P. (2020). Nanoscale Self-Assembly for Therapeutic Delivery. *Front Bioeng Biotechnol*, 8, 127. doi:10.3389/fbioe.2020.00127.

Zou, Q., Abbas, M., Zhao, L., Li, S., Shen, G., and Yan, X. (2017). Biological Photothermal Nanodots Based on Self-Assembly of Peptide–Porphyrin Conjugates for Antitumor Therapy. *Journal of the American Chemical Society*, 139(5), 1921-1927. doi:10.1021/jacs.6b11382.





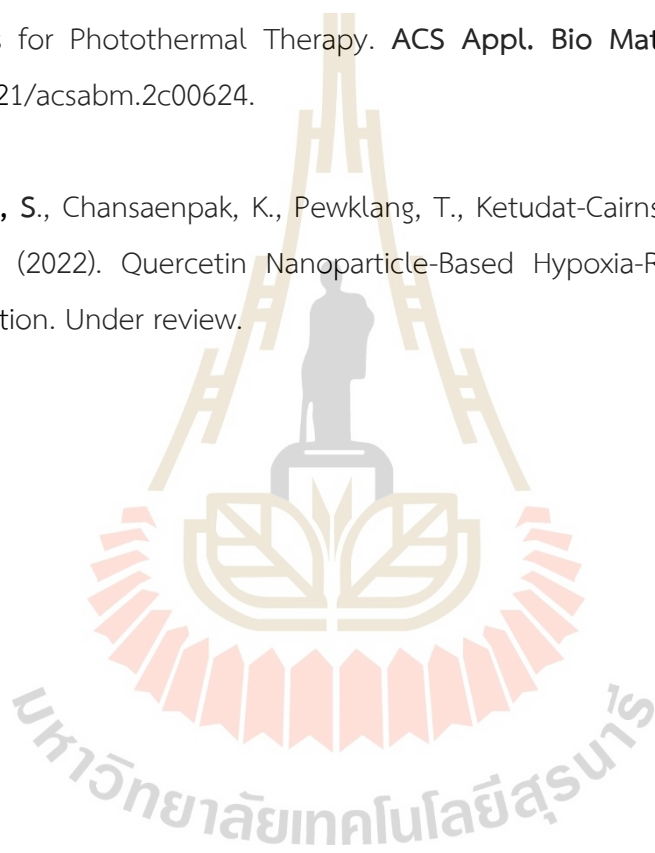
APPENDIX

APPENDIX

THESIS OUTPUT

Kampaengsri, S., Chansaenpak, K., Yong, G. Y., Hiranmartsuwan, P., Uengwanarat, B., Lai, R. Y., Meemon, P., Kue C, S., and Kamkaew, A. (2022). PEGylated Aza-BODIPY Nanoparticles for Photothermal Therapy. *ACS Appl. Bio Mater.* 5, 9, 4567–4577: doi.org/10.1021/acsabm.2c00624.

Kampaengsri, S., Chansaenpak, K., Pewklang, T., Ketudat-Cairns, J. R., Lai, R. Y., and Kamkaew, A. (2022). Quercetin Nanoparticle-Based Hypoxia-Responsive Probe for Cancer Detection. Under review.



CURRICULUM VITAE

Name Sastiya Kampaengsri

Date of Birth August 20th, 1993 at Nong Bua Lamphu, Thailand

Education

- 2019 to present Ph.D. in Chemistry, (PEGylated Aza-BODIPY Nanoparticles for Photothermal Therapy) Under the Supervision of Assist. Pro. Dr. Anyanee Kamkaew, School of Chemistry, Institute of Science, Suranaree University of Technology, Thailand (expected 2022).
- 2017 to 2019 M.Sc. in Chemistry, (Gold sensing with rhodamine immobilized Hydrogel-based colorimetric sensor) Under the supervision of Assoc. Prof. Dr. Chatthai Kaewtong, Department of Chemistry, Faculty of Science, Maharakham University, Maharakham, 44150, Thailand.
- 2012 to 2016 B.Sc. in Chemistry under the supervision of Assoc. Prof. Dr. Chatthai Kaewtong, Department of Chemistry, Faculty of Science, Maharakham University, Maharakham, 44150, Thailand.

Work experience

- 22/7/2562 - 28/9/2562 Researcher in Institute of Beauty and Health Sciences, responsible for high performance of ingredient synthetic in cosmetics.

Conferences and presentations

- 4/7/2561 - 7/7/2561 PERCH-CIC Congress X: 2018 International Congress for Innovation in Chemistry
- 20/1/2563 – 21/1/2563 Pure and Applied Chemistry International Conference

Grants

- 2559-2562 Center for Innovation in Chemistry (PERCH-CIC)
- 2562-2565 Thailand Science Research and Innovation (TSRI)